Lappeenranta-Lahti University of Technology LUT
School of Engineering Science
Computational Engineering and Technical Physics
Technomathematics

Aleksandr Zinovev

UNCERTAINTY QUANTIFICATION OF FAIR CLIMATE MODEL

Master's Thesis

Examiners: Heikki Haario, Lassi Roininen

Supervisors: Heikki Haario

ABSTRACT

Lappeenranta-Lahti University of Technology LUT
School of Engineering Science
Computational Engineering and Technical Physics
Technomathematics

Aleksandr Zinovev

UNCERTAINTY QUANTIFICATION OF FAIR CLIMATE MODEL

Master's Thesis

2020

61 pages, 23 figures, 5 table, 1 appendix.

Examiners: Heikki Haario, Lassi Roininen

Keywords: Markov chain Monte Carlo, FaIR model, climate model, sensitivity analysis, X-Degree Compatibility model.

The FaIR model is a simple climate–carbon-cycle model. It is used for the estimation of temperature change caused by greenhouse gas emissions. The objective of the thesis was the conduction of sensitivity analysis of the FaIR model by using the Markov chain Monte Carlo method and estimation of posterior distributions of 20 internal FaIR parameters. That allowed to estimate the FaIR output uncertainties. The other sources of error (for example uncertainties of the input data) are not considered. The results of the work show improvement of the error estimation comparing to the results calculated by the simple Monte-Carlo method by using the prior distributions of the parameters. In addition, an example use-case is presented as an error validation of the X-Degree Compatibility model which is an economic climate impact model that uses FaIR.

PREFACE

I would like to thank my supervisors Heikki Haario and Jacopo Pellegrino for their useful comments during the preparation of this work.

Lappeenranta, June 20, 2021

Aleksandr Zinovev

CONTENTS

LIST OF ABBREVIATIONS

AM	Adaptive Metropolis
DR	Delayed Rejection
DRAM	Delayed Rejection Adaptive Metropolis
ERF	Effective Radiative Forcing
ESM	Earth System Models
FaIR	Finite Amplitude Impulse Response
GHG	Greenhouse gas
MCMC	Markov chain Monte Carlo
MH	Metropolis Husting
RF	Radiative Forcing
XDC	X-Degree Compatibility

1 INTRODUCTION

1.1 Background

Prediction of temperature change is essential for estimation of the carbon cost, the effectiveness of social policies, and risks associated with climate change [6]. The future temperature is heavily dependent on carbon dioxide emissions (CO_2) [5]. Therefore, Earth System Models (ESMs), complex models that simulate physical processes that govern the interaction between climate and carbon cycle, are used in order to predict temperature change. ESMs are complex models that require an extensive amount of computational power and, therefore, they are usually used only for few representative scenarios. Hence, simple climate–carbon-cycle models can be necessary for some use-cases (for example, when large amount of computational power is absent) and a number of such models were suggested [6, 8].

The Finite Amplitude Impulse Response (FaIR) model is one of the suggested simple climate–carbon-cycle models that was first introduced in the paper by Millar et al. in 2017 [6] and originally considered only CO_2 emission. In 2018 advanced version of the model was proposed by Smith et al. [8] that considers the concentrations of a set of 31 greenhouse gases (GHG) including CO_2 and 13 different effective radiative forcings (ERF) groups which are caused by different gases and phenomenons.

The FaIR model calculates approximative prediction. The uncertainties of the FaIR's parameters and inputs (for example GHG emission) are the cause of the output variability. Estimation of this uncertainty is important for the same reasons why prediction of climate change is essential. It also allows to an evaluation of risks associated with the rise of temperature.

1.2 Objectives and delimitations

In Smith's article [8] a simple uncertainty analysis of the FaIR model was conducted. A set of 21 FaIR parameters and their priors was used in the Monte Carlo simulation to estimate the model's uncertainty.

The objective of this work was to conduct deeper uncertainty analysis and estimate posterior distribution of the model variables and by that narrowing uncertainty of FaIR's

output. In order to do that Markov chain Monte Carlo method was used with the set of temperature output of 11 different ESM models were used.

In this work we are restricted with only uncertainty caused by a limited set of FaIR parameters and not with uncertainties of the FaIR's input such as GHG emission and solar and volcanic radiative forcing.

1.3 Structure of the thesis

This work makes short introduction into FaIR model and MCMC method in Section 2. Section 3 then discusses the experiments that was conducted as well as discription of the set of the parameters that are used in MCMC generation and temperature dataset. Finaly, the results are discussed in Section 4.

2 METHODS

This Section makes a short introduction to the FaIR model and Markov chain Monte Carlo method which was used in this work.

2.1 FaIR

Prediction of climate change requires a complex model that simulates the interaction between climate and the carbon cycle. Comprehensive ESMs are explicitly modelling physical processes, coupled evolution of CO_2 concentration, and temperature response. The main downside of ESMs is their complexity and requirement of a significant amount of computations. Consequentially, they are usually used for simulating a few representative emission scenarios [6].

A number of simple climate–carbon-cycle models were suggested in order to calculate temperature change without the necessity of long simulation time. This type of the models are deliberately designed to simulate the behaviour of ESMs [6].

FaIR was first introduced in 2017 by Millar et al. [6] and is a simple climate–carbon-cycle model. It is an extension of the standard IPCC AR5 impulse response model (AR5-IR). The main difference between FaIR and AR5-IP is the ability of FaIR to simulate two phenomenons that are important features of ESM's behaviour: negative impact of high temperature on the ability of carbon sinks to absorb CO_2 and ability of increase of airborne CO_2 fraction to effect relationship between CO_2 concentration and radiative forcing. These two features are essential for simulation of Earth's response to impulse emission. Therefore, FaIR shows results closer to fully coupled ESM than other simple models as AR5-IR or PI-IR [6].

Later, in 2018, a new advanced version of FaIR (also known as FaIR 1.3) was suggested by Smith et al. [8]. The differences between the models, according to Smith, are:

> FAIR v1.0 is well-calibrated to the temperature and carbon cycle response of earth system models. FAIR v1.3 is extended to calculate non-CO_2 greenhouse gas concentrations from emissions, aerosol forcing from aerosol precursor emissions, tropospheric and stratospheric ozone forcing from the emissions of precursors, and forcings from black carbon on snow, stratospheric

> methane oxidation to water vapour, contrails and land use change. Forcings from volcanic eruptions and solar irradiance fluctuations are supplied externally. These forcings are then converted to a temperature change, taking into account the different thermal responses of the ocean mixed layer and deep ocean. (p. 2274)

A brief introduction to FaIR 1.3 is presented below with a general algorithm shown on fig. 1. For more detail see the original article by Smith et al. [8].

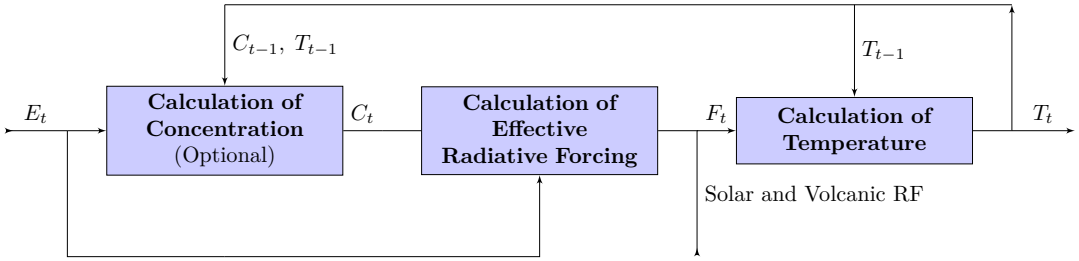

Figure 1. General flowchart of the FaIR algorithm. FaIR's inputs are GHG emissions as well as solar and volcanic radiative forcings. Temperature and concentration updated each step. The timestep of the model is one year.

Primarily, the FaIR model's inputs are the emission of GHG gases (natural and anthropogenic) and volcanic and solar radiative forcing time-series that have to be provided externally. The model has a high degree of variability and some inputs can be added or changed (for example, GHG concentration can be used instead of emission), but in this work, the case that was just described is presented and used.

As was mentioned in the quote, FaIR 1.3 sequentially calculates concentration, effective radiative forcing (ERF), and temperature for each time step. Therefore the algorithm can be divided into three corresponding parts: calculation of concentration, calculation of effective radiative forcing, and calculation of temperature.

2.1.1 Calculation of concentration

The calculation of GHG concentration is an optional step and can be skipped in the case if the concentration time-series is provided instead of emission time-series. During this

Table 2. List of GHG gases used in the FaIR m

Index	Gas	Index	Gas	Index	Gas
0	CO_2	11	HFC143a	22	HCFC22
1	CH_4	12	HFC227ea	23	HCFC141b
2	N_2O	13	HFC245fa	24	HCFC142b
3	CF_4	14	SF_6	25	Halon 1211
4	C_2F_6	15	CFC11	26	Halon 1202
5	C_6F_{14}	16	CFC12	27	Halon 1301
6	HFC23	17	CFC113	28	Halon 2402
7	HFC32	18	CFC114	29	CH_3Br
8	HFC43-10	19	CFC115	30	CH_3Cl
9	HFC125	20	CCl_4		
10	HFC134a	21	Methyl chloroform		

step, FaIR updates the concentration of a set of 31 GHG (table 2) with respect to their emission and decay.

Simulation of a carbon cycle have a special importance since CO_2 concentration have considerable influence on the climate [5, 6]. In order to simulate a CO_2 absorption by different Earth systems, four-box decay model is used. The boxes (also known as reservoirs or pools) represent a combination of various carbon-cycle mechanisms and correspond to geological, deep ocean, biosphere, and ocean mixed layer processes. Anthropogenic CO_2 emission is distributed into four boxes R_i according partial fractions a_i ($\sum_{i=1}^{4} a_i = 1$). Governing equation for each reservoir is

$$\frac{\mathrm{d}R_i}{\mathrm{d}t} = a_i E_{\mathrm{CO_2}} - \frac{R_i}{\alpha\tau_i};\ i = 1, ..., 4, \tag{1}$$

where $E_{\mathrm{CO_2}}$ is the emission of CO_2, τ_i is the lifespan of the CO_2 in the box i, and α is a coefficient that depends on temperature and all-time cumulative CO_2 emission. It is determined from solving a non-linear equation that is composed of two different governing equations for 100-year integrated impulse response function iIRF_{100}:

$$\sum_{i=1}^{4} \alpha a_i \tau_i \left[1 - \exp\left(\frac{-100}{\alpha\tau_i}\right)\right] = r_0 + r_{\mathrm{C}} C_{\mathrm{CO_2,acc}} + r_{\mathrm{T}} T. \tag{2}$$

Here, $C_{\mathrm{CO_2,acc}}$ is total accumulated carbon in land and ocean ($C_{\mathrm{CO_2,acc}} = (\sum_t E_{\mathrm{CO_2},t}) - (C_{\mathrm{CO_2}} - C_{\mathrm{CO_2,pi}})$, where pi means 'pre-industrial') and T is temperature change since

pre-industrial era. Overall $\mathrm{CO_2}$ concentration $C_{\mathrm{CO_2}}$ is calculated as

$$C_{\mathrm{CO_2}} = C_{\mathrm{CO_2,pi}} + \sum_{i=1}^{4} \frac{R_i}{M_a} \frac{w_a}{w_{\mathrm{CO_2}}}, \tag{3}$$

where $M_a = 5.1352 \times 10^{18}$ – dry mass of atmosphere, w_a and w_{f} are molecular mass of dry air and the $\mathrm{CO_2}$ respectively.

For all the other GHG, one-box decay model is used. The calculation is done in two steps. First step is conversion of the gas emission E_t to an increase of the gas concentration δC_t by using

$$\delta C_t = \frac{E_t}{M_a} \frac{w_a}{w_{\mathrm{f}}} \delta_t, \tag{4}$$

where δ_t – time step in years. Then, the concentration of the gas C_t is calculated with respect to decay and the increase:

$$C_t = C_{t-1} + \frac{1}{2}(\delta C_{t-1} + \delta C_t) - C_{t-1}(1 - \exp(-1/\tau)), \tag{5}$$

where τ is an atmospheric lifetime for the gas.

The FaIR model also takes into account methane oxidation. Approximately 61% of fossil $\mathrm{CH_4}$ is converted to $\mathrm{CO_2}$ what is an additional source of $\mathrm{CO_2}$ emission:

$$E_{\mathrm{CH_4 \to CO_2}} = 0.61 f_{\mathrm{CH_4 fos}}(C_{\mathrm{CH_4}} - C_{\mathrm{CH_4,pi}})(1 - \exp(-1/\tau_{\mathrm{CH_4}})). \tag{6}$$

The flowchart of this calculation of concentration step is presented on fig. 2.

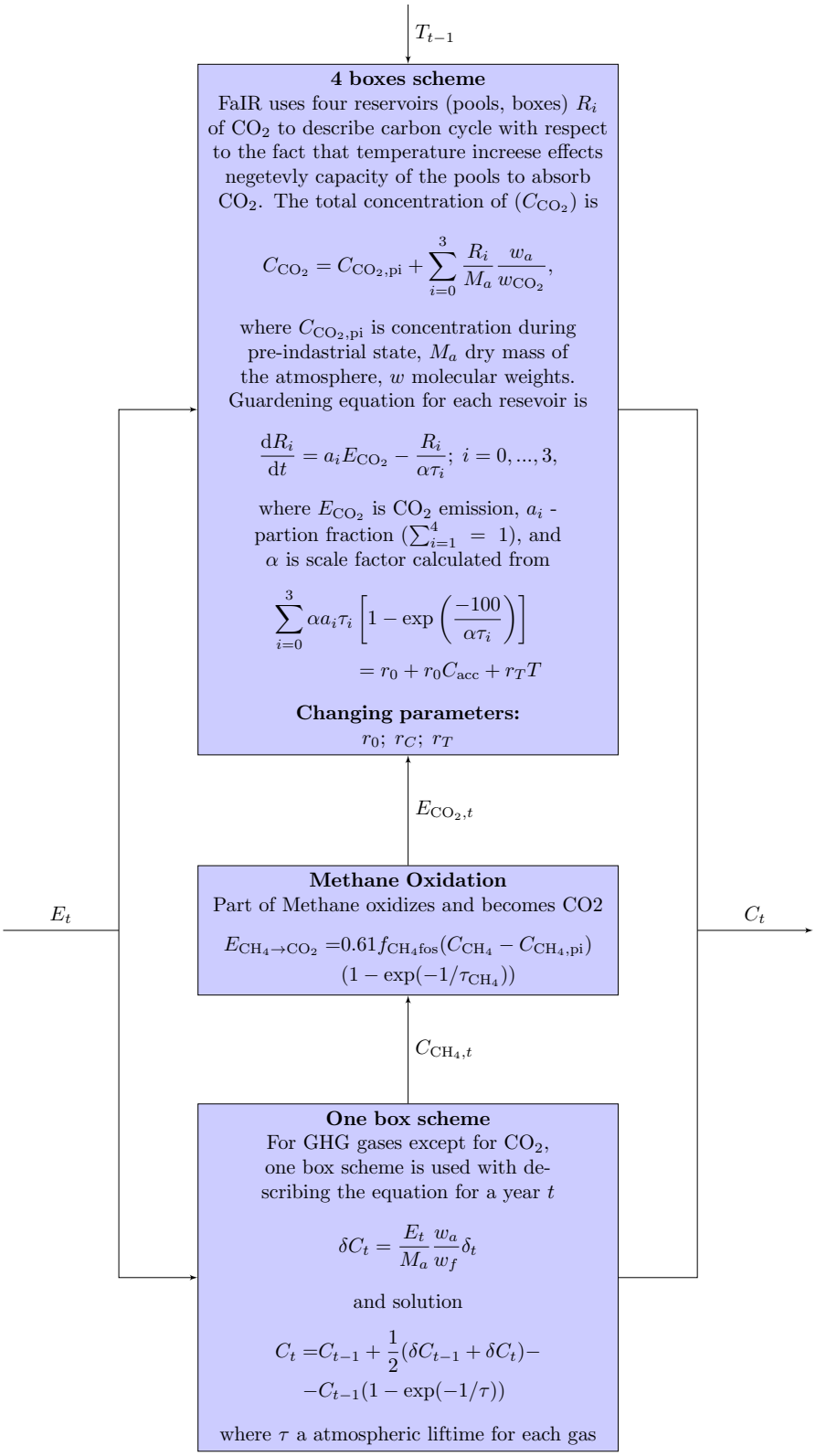

Figure 2. Calculation of concentration flowchart

2.1.2 Calculation of effective radiative forcing

The second part is the estimation of ERF and Radiative Forcing (RF) caused by GHG and the other effects (the flowchart of the step is presented on figs. 4 and 5). The concept of RF has been applied for many years and used as a metric for comparing the impact of various mechanisms on Earth's radiation imbalance. The ERF is an extended version of RF [7] that not only accounts for stratospheric rapid adjustments (as RF does) but also includes tropospheric ones [8]. Since ERF better corresponds to the temperature change, FaIR uses estimations of ERF when it is possible.

Overall, FaIR estimates 13 separate forcing groups caused by different gases and phenomenons: CO_2, CH_4, N_2O, other GHG, tropospheric ozone, stratospheric ozone, stratospheric water vapour, contrails, aerosols, black carbon on snow, land-use change, volcanic, and solar.

Governing equations from Etminan et al. [1] are used in FaIR for calculations of ERFs caused by CO_2, CH_4, and N_2O. These gases have overlaps between wavelengths of radiations that are absorbed by them. Therefore ERF of each gas is calculated with respect to the concentrations of itself and the others:

$$\begin{aligned} F_{\mathrm{CO_2}} = \big[&(-2.4\times10^{-7})(C-C_{\mathrm{pi}})^2 + (7.2\times10^{-4})|C-C_{pi}| \\ &- (1.05\times10^{-4})(N+N_{\mathrm{pi}}) + 5.36\big] \times \log\left(\frac{C}{C_{\mathrm{pi}}}\right), \end{aligned} \tag{7}$$

$$\begin{aligned} F_{\mathrm{N_2O}} = \big[&(-4.0\times10^{-6})(C+C_{\mathrm{pi}}) + (2.1\times10^{-6})(N+N_{\mathrm{pi}}) \\ &- (2.45\times10^{-6})(M+M_{\mathrm{pi}}) + 0.117\big] \times \log\left(\sqrt{N}-\sqrt{N_{\mathrm{pi}}}\right), \end{aligned} \tag{8}$$

$$\begin{aligned} F_{\mathrm{CH_4}} = \big[&(-6.5\times10^{-7})(M+M_{\mathrm{pi}}) - (4.1\times10^{-6})(N+N_{\mathrm{pi}}) + 0.043\big] \\ &\times \log\left(\sqrt{M}-\sqrt{M_{\mathrm{pi}}}\right) \end{aligned}, \tag{9}$$

where C,M,N concentrations of CO_2, CH_4, N_2O respectively and measured in ppm for CO_2 and ppb for the others.

In addition, $F_{\mathrm{CO_2}}$ is scaled to make sure that ERF calculated by eq. (7) on condition of doubling of CO_2 is equal to $F_{2\times} = 3.71\ \mathrm{Wm^{-2}}$.

Figure 3 shows ERF calculated according to eqs. (7) to (9). The minimum and maximum of GHG concentrations are chosen from the output of FaIR with default parameters and RCP 8.5 emission scenario (see Section 3.4.1 for details). Minimum values approxi-

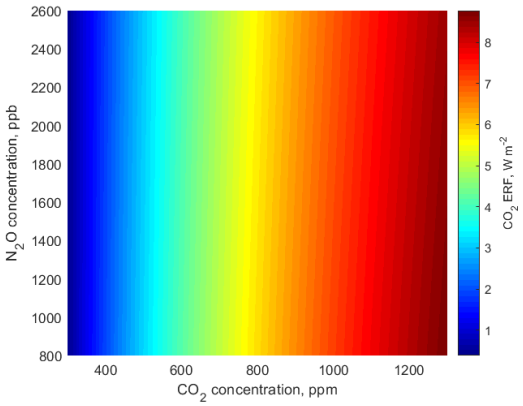

(a) CO_2

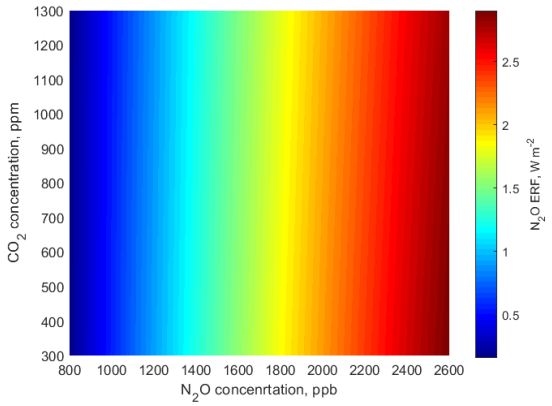

(b) N_2O. Methane concentration 280 ppb;

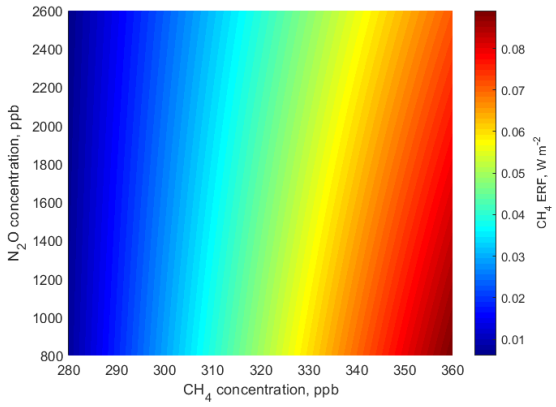

(c) CH_4

Figure 3. Efective radiative forcings of the carbon dioxide, nitrous oxide, and methane according to eqs. (7) to (9).

mately correspond to the pre-industrial concentrations and the maximum values – to the concentration by the year 2050.

While forcing of the $\mathrm{CO_2}$ and $\mathrm{CH_4}$ depends on concentrations of two gases, the ERF of the $\mathrm{N_2O}$ depends on three concentrations and therefore fig. 3b depicts the case with fixed methane concentration. In addition, methane concentration insignificantly affects the overall $\mathrm{N_2O}$ ERF: term of eq. (8) that depends on methane concentration $((2.45 \times 10^{-6})(M + M_{\mathrm{pi}}))$ is equal to 0.0014 if $M = 280$ and to 0.0016 if $M = 360$, while the minimum forcing (fig. 3b) is $0.1591\ \mathrm{Wm^{-2}}$.

The charts show expected tendencies. The rise of the GHG increases the ERF caused by the corresponding gas. Withal, the concentration of the other gases reduces the forcing due to the overlap of wavelengths of absorbed radiation.

ERFs of other well-mixed GHG (gases with indexes $3, ..., 30$ in table 2) are assumed to be a linear function of the gas concentration

$$F_i = \eta_i(C_i - C_{i,\mathrm{pi}}), \tag{10}$$

where η_i is coefficient unique for every gas.

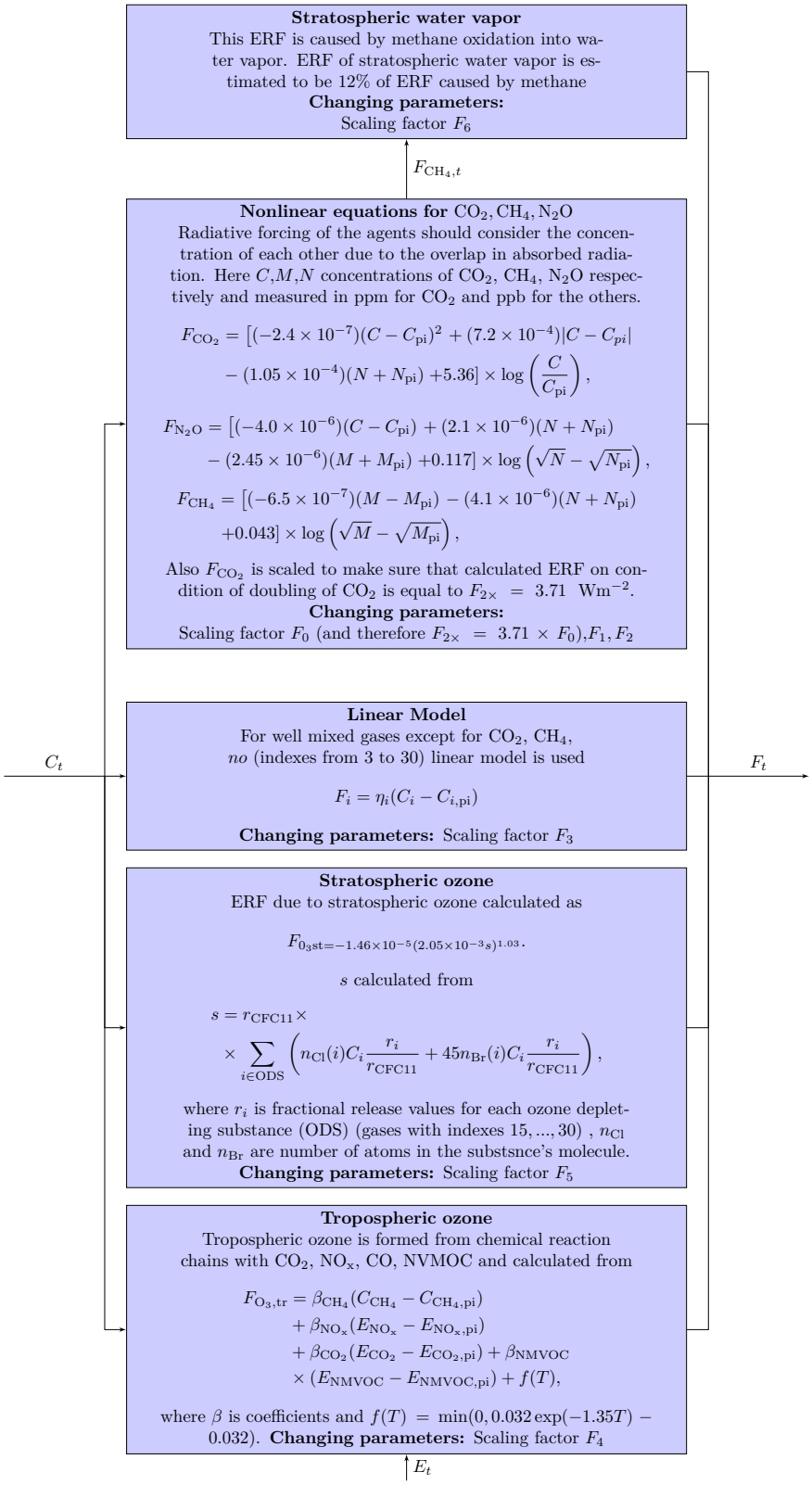

Figure 4. Calculation of effective radiative forcing from GHG concentrations and emissions flowchart

Since the tropospheric ozone has a short lifespan and it's concentration is not uniform neither constant, its radiative forcing is calculated directly without calculation of the concentration. The tropospheric ozone is a product of chemical reaction caused by $\mathrm{CH_4}$, $\mathrm{NO_x}$, CO, and NVMOC, and it's ERF is estimated from the emission and concentration of the gases involved in the reaction chain:

$$\begin{aligned} F_{\mathrm{O_3,tr}} = \beta_{\mathrm{CH_4}}(C_{\mathrm{CH_4}} - C_{\mathrm{CH_4,pi}}) + \beta_{\mathrm{NO_x}}(E_{\mathrm{NO_x}} - E_{\mathrm{NO_x,pi}}) + \\ + \beta_{\mathrm{CO_2}}(E_{\mathrm{CO_2}} - E_{\mathrm{CO_2,pi}}) + \beta_{\mathrm{NMVOC}}(E_{\mathrm{NMVOC}} - E_{\mathrm{NMVOC,pi}}) + f(T), \end{aligned} \tag{11}$$

where β is coefficients and $f(T) = \min(0, 0.032\exp(-1.35T) - 0.032)$.

Stratospheric ozone's ERF is estimated from

$$F_{0_3,\mathrm{st}} = -1.46 \times 10^{-5}(2.05 \times 10^{-3}s)^{1.03} \tag{12}$$

with s determined from

$$s = r_{\mathrm{CFC11}} \sum_{i \in \mathrm{ODS}} \left(n_{\mathrm{Cl}}(i) C_i \frac{r_i}{r_{\mathrm{CFC11}}} + 45 n_{\mathrm{Br}}(i) C_i \frac{r_i}{r_{\mathrm{CFC11}}} \right), \tag{13}$$

where r_i is fractional release values for each ozone depleting substance (ODS) (gases with indexes $15, ..., 30$) , n_{Cl} and n_{Br} are number of atoms in the substsnce's molecule.

The ERF due to stratospheric water vapor is estimated as 12% of the methane ERF.

The ERF caused by aviation via contrails can be estimated in three different ways in the FaIR model. By default, without additional input, the linear model is used, where forcing is scaled according to aviation $\mathrm{NO_x}$ emission growth:

$$F_{\mathrm{con}} = \frac{E_{\mathrm{NO_x,avi}}}{E_{\mathrm{NO_x,avi2005}}} F_{\mathrm{con,2005}}. \tag{14}$$

Aviation $\mathrm{NO_x}$ emission is considered to be fraction of total $\mathrm{NO_x}$ emission.

Aerosols contribute to climate change in two different ways: via aerosol-radiation interaction and via aerosol-cloud interaction. ERF due to aerosol-radiation interaction estimated by

$$\begin{aligned} F_{\mathrm{ari}} = \gamma_{\mathrm{BC}} E_{\mathrm{BC}} + \gamma_{\mathrm{OC}} E_{\mathrm{OC}} + \gamma_{\mathrm{SO_x}} E_{\mathrm{SO_x}} + \\ + \gamma_{\mathrm{NH_3}} E_{\mathrm{NH_3}} + \gamma_{\mathrm{SOA}} E_{\mathrm{NMVOC}} \end{aligned} \tag{15}$$

where γ are constant coefficients. And for aerosol-cloud radiation

$$F_{\text{aci}} = -0.45\frac{G(E) - G(E_{1765})}{G(E_{2011}) - G(E_{1765})}, \tag{16}$$

where

$$G(E_{\text{SO}_\text{x}}, E_{\text{BC+OC}}) = -1.95\log(1 + 0.0111E_{\text{SO}_\text{x}} + 0.0139E_{\text{BC+OC}}) \tag{17}$$

and $G(E) = G(E_{\text{SO}_\text{x}}, E_{\text{BC+OC}})$.

The ERF caused by black carbon on snow is determined from the black carbon emission:

$$F_{\text{BCsnow}} = 0.00494E_{\text{BC}}. \tag{18}$$

To estimate ERF due to change in the Earth albedo caused by anthropogenic activity the cumulative sum of land-use CO_2 emission is used

$$F_{\text{landuse}} = -1.14 \times 10^{-3}\sum_{j=0}^{t} E_{\text{CO}_2\text{land},j} \tag{19}$$

As will be discussed later in Section 3.1, the scaling factors of the forcings groups are used as sampled variables instead of the forcings themselves. Correspondence of the scaling factors to the groups shown in table 4.

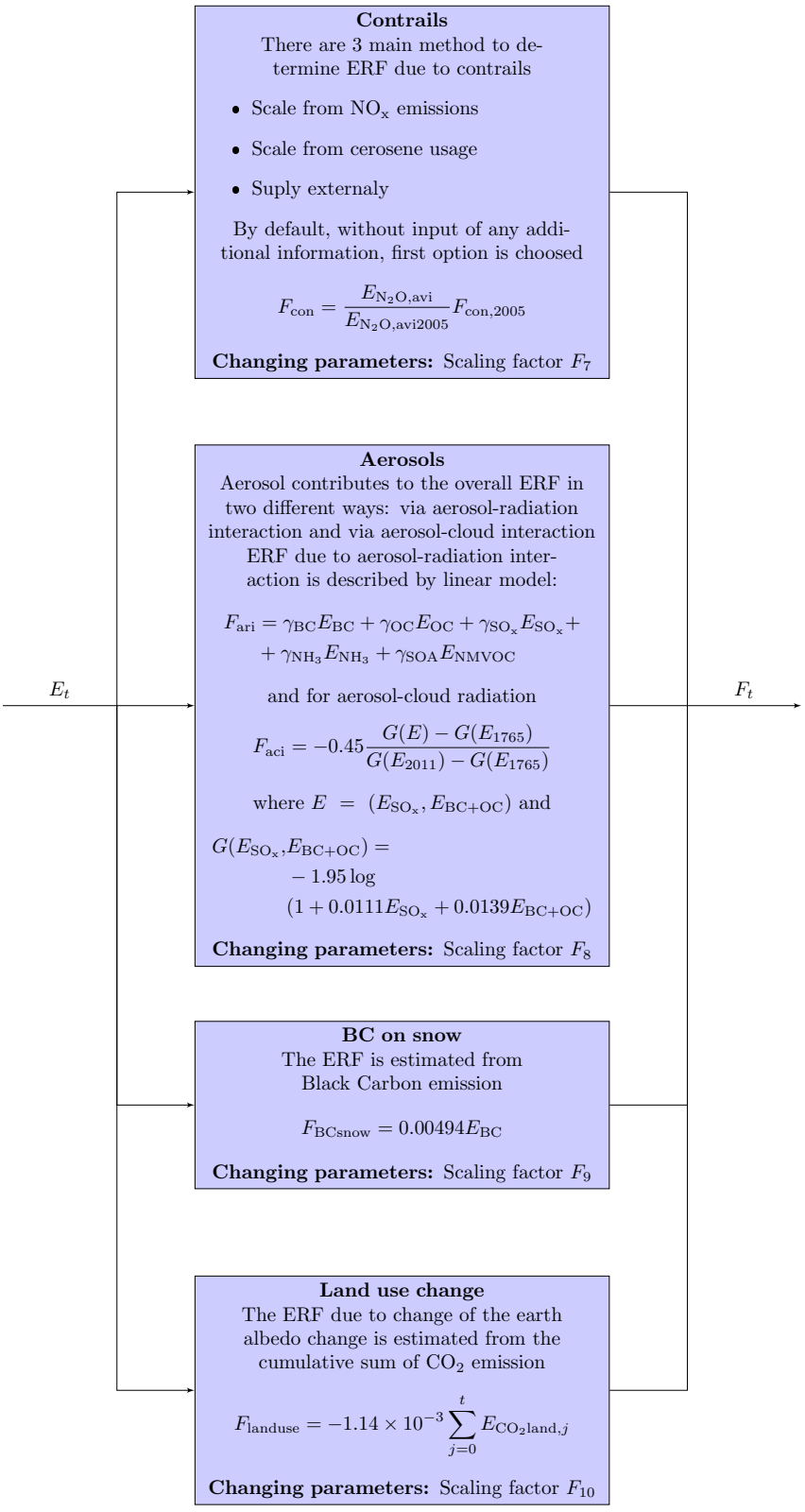

Figure 5. Calculation of effective radiative forcing from GHG emissions flowchart

2.1.3 Calculation of temperature

Temperature change is described by two constant temperature model, where the total temperature change depends on the sum of of the radiative forcings:

$$T_{t,i} = T_{t-1,i} \exp(1/d_i) + \sum_{j \in \mathrm{G}} (q_i \epsilon_j F_j (1 - \exp(1/d_i))); \tag{20}$$

where $i = 1, 2$, G is the set of all forcing groups described in 2.1.2 (such as CO_2, volcanic, etc.), ϵ_j is efficacy of the forcing j, d_i describe slow ($i = 1$) and fast ($i = 2$) ocean response for temperature change, q_i are coefficient derived from

$$T_{\mathrm{ECS}} = F_{2\times}(q_1 + q_2) \tag{21}$$

$$T_{\mathrm{TCR}} = F_{2\times}\left(q_1\left(1 - \frac{d_1}{D}\left(1 - \exp\left(-\frac{D}{d_1}\right)\right)\right) + q_2\left(1 - \frac{d_2}{D}\left(1 - \exp\left(\frac{D}{d_2}\right)\right)\right)\right) \tag{22}$$

The total temperature change is calculated as $T_t = T_{t,1} + T_{t,2}$.

The flowchart of this step is depicted on fig. 6.

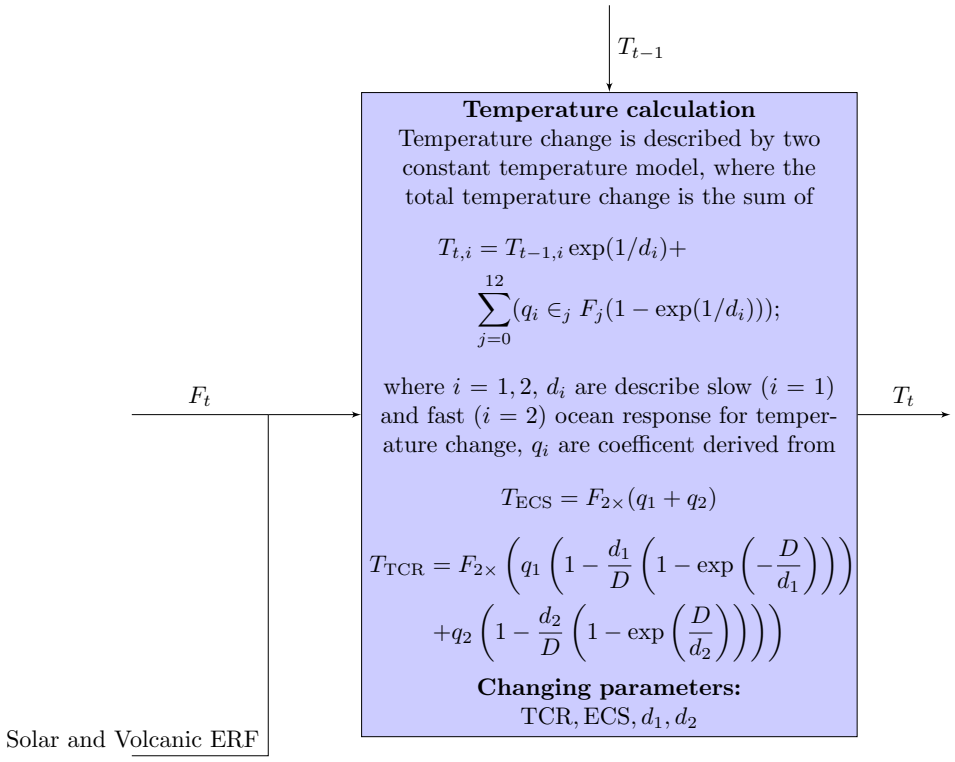

Figure 6. Calculation of temperature flowchart

2.2 X-Degree Compatibility Model

The X-Degree Compatibility (XDC) model is an economic climate impact model. The result of the model is the temperature change in degrees Celsius since the pre-industrial period provided that the entire world operated with identical emission intensity as an economical entity under consideration over a given period between base and target years. The XDC model can be used to calculate the climate impact not only of listed companies, but also of other economic entities such as sovereing bonds or private equities. The following description is based on the assumption that the model is dealing with a public company for simplicity.

There are four XDC metrics: Baseline XDC, Sector XDC, Target XDC, and Scenario Based XDC. Baseline XDC is used for estimating economical entities' impact on climate change during its usual performance. Sector XDC is used for estimating an economic sector's contribution to climate change. Target XDC is the temperature threshold that all economical entities of a particular sector must be aligned to achieve the goal of global warming defined by a given target scenario. Each target scenario has a target temperature

and is based on specific assumptions regarding future developments. Among the others, B2DS (Below 2 Degree Scenario) and 2DS (2 Degree Scenario) from IEA are used for target temperatues of respectively $1.75\mathrm{C}^{\circ}$ and $2.0\mathrm{C}^{\circ}$. Target XDC varies between sectors since emission intensity depends on the nature of the economic activity. Scenario XDC allows for a custom strategy for economical and emission growth instead of using baseline growth rates.

The following data is used in XDC calculation for companies: gross value added (GVA) and GHG emission for scopes 1, 2, and 3 of the entities under consideration in the base year; global GVA; the growth rate of the entities emission and GVA; the growth rate of global GVA. Assumptions about the growths in the case of Baseline XDC depend on the country and region in which the economic entity is located.

XDC uses described data for calculation of hypothetical CO_2 emissions and uses them as an input to the FaIR model.

The hypothetical emissions are calculated in two steps. The first step is determining the economic emission intensity (EEI) of the economical entity. EEI is defined as GHG emission as CO_2 equivalent per million Euro gross value added and calculated for each year:

$$\mathrm{EEI}_{\mathrm{i,k}} = e_{i,k}/\mathrm{GVA}_k;\ k = b_y, ..., t_y;\ i = 1, ..., 3, \tag{23}$$

where b_y stand for base year, t_y - for target year, and $e_{i,k}$ is scope i emission of the economical entities during year k. A weight of 50% is applied to scopes 2 and 3 of the reported emission in the case of Baseline XDC since these emissions contribute to the GVA of other entities.

The second step is to scale the CO_2 emission E along global GVA:

$$E_{i,k} = \mathrm{EEI}_{\mathrm{i,k}} \times \mathrm{GVA}_{\mathrm{Glob},k}. \tag{24}$$

The total global theoretical emission is a sum of the emissions of scopes 1, 2, 3:

$$E_{\mathrm{tot.},k} = \sum_{i}^{\mathrm{Scopes}} E_{i,k} \tag{25}$$

2.3 Markov chain Monte Carlo

Let us consider a non-linear model

$$\mathbf{y} = f(\mathbf{x}|\theta) + \epsilon, \tag{26}$$

where $\mathbf{y}$ are the measurements, f is a non-linear function with parameters θ and design variables $\mathbf{x}$, and ϵ is noise. Due to the noise, it is impossible to estimate θ with a total precision but it is possible to calculate the probability distribution of θ.

For this non-linear model, Bayes' theorem can be written as

$$p(\theta|\mathbf{y}) = \frac{p(\mathbf{y}|\theta)p(\theta)}{\int p(\mathbf{y}|\theta)p(\theta)\,d\theta}\ , \tag{27}$$

where $p(\theta|\mathbf{y})$ is posterior distribution of the parameter θ given the observation $\mathbf{y}$, $p(\mathbf{y}|\theta)$ is a likelihood of $\mathbf{y}$ occurring given the parameter values are θ, $p(\theta)$ is a prior distribution of θ, the integral is a normalization constant and equal to the prior distribution $p(\mathbf{y})$.

In other words, to obtain information regarding of probability distribution of parameter θ with respect to obtained measurements $\mathbf{y}$, information about the prior distribution of $\mathbf{y}$ and θ is needed as well as the likelihood of $\mathbf{y}$ occurring if parameter θ is given. Prior distribution of $\mathbf{y}$ can be calculated ($p(\mathbf{y}) = \int p(\mathbf{y}|\theta)p(\theta)\,d\theta$) but the integration can require intensive calculation, especially in the case with more then few parameters when integral became an multiple one.

Markov chain Monte Carlo (MCMC) is a method that allows sampling a posterior distribution by generating a sequence (chain) $(\theta_i)_{i=1}^{N}$ which asymptotically approaches the posterior distribution. The chain is generated randomly (from which the term 'Monte Carlo' is used) and every member except the first depends only on the previous member (from which the term 'Markov chain' is used). The main advantage of MCMC is ability to sample posterior distribution (in this case $p(\theta|\mathbf{y})$) without computing a multidimensional integral ($\int p(\mathbf{y}|\theta)p(\theta)\,d\theta$).

Several algorithms exist to generate a MCMC chain. One of the most used is Metropolis Husting (MH) algorithm [10]. It starts with the initial point θ_1 and repeating the following steps until the chain of required length is generated (the distribution of the sequence is close to the posterior distribution):

- Choose a candidate $\hat{\theta}$ with respect to proposal distribution $q(\hat{\theta}, \theta_n)$
- Accept the candidate with probability

$$\alpha(\theta_n, \hat{\theta}) = \min\left(1, \frac{p(\hat{\theta})q(\theta_n, \hat{\theta}))}{p(\theta_n)q(\hat{\theta}, \theta_n)}\right) \tag{28}$$

If proposal distribution is a symmetric one (which means that $q(\hat{\theta}, \theta) = q(\theta, \hat{\theta})$) the method is called 'Metropolis algorithm'.

The choice of the proposal distribution affects the speed of convergence and varies from case to case. Often multivariate normal distribution is used as a proposal one and then the choice of the covariance matrix can heavily influence the optimal length of the chain and therefore time of calculation. To deal with that problem Adaptive Metropolis (AM) algorithm can be used [3].

The main idea of the AM is to update the covariance matrix during the chain generation. After the initial covariance matrix C_0 is proposed the chain is generated until the n_0-th member (so-called 'burn-in' period) and then every few steps update the covariance. For the case with update every turn the formula is

$$C_n = \begin{cases} C_0, & n < n_0 \\ s_d \mathrm{Cov}(\theta_0, ..., \theta_{i-1}) + s_d \epsilon \mathbf{I}_d, & n \geq n_0, \end{cases} \tag{29}$$

where s_d is a scaling parameter that depends on number of dimensions d and usually set to $s_d = 2.4^2/d$, and ϵ is a small positive constant to ensure that C_n not became singular. See fig. 7 for the algorithm flowchart.

Another advanced method is Delayed Rejection (DR) algorithm. The method is the same as MH except in the case of rejection of an candidate $\hat{\theta}^{(1)}$ second candidate $\hat{\theta}^{(2)}$ is generated from the other proposal distribution $q_2(\hat{\theta}^{(2)}, \hat{\theta}^{(1)}, \theta_n)$ with respect to the rejected candidate. Probability of acceptance is

$$\alpha_2(x, y_1, y_2) = \min\left(1, \frac{p(y_2)q_1(y_2, y_1)q_2(y_2, y_1, x)[1 - \alpha_1(y_2, y_1)]}{p(x)q_1(x, y_1)q_2(x, y_1, y_2)[1 - \alpha_1(x, y_1)]}\right), \tag{30}$$

where α_1 is calculated from eq. (28). The process can be continued by generating others candidates with respect to the rejected ones or stopped and then, as in the MH algorithm, the next chain member is setted as the current one ($\theta_{n+1} = \theta_n$). See fig. 8 for the flowchart.

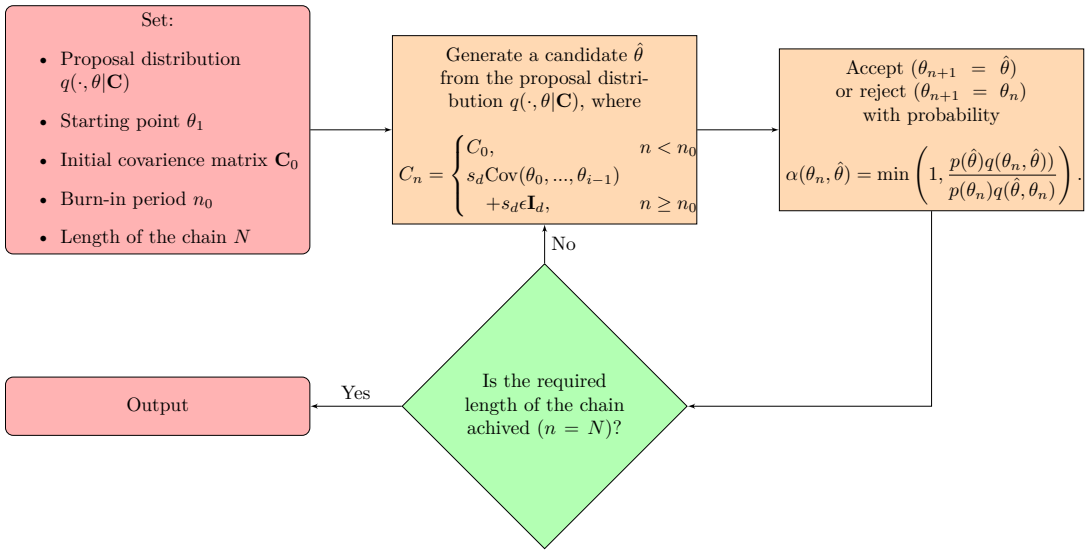

Figure 7. Adaptive Metropolis Algorithm with an update of covariance matrix every step

The combination of the mentioned above method is Delayed Rejection Adaptive Metropolis (DRAM) algorithm [4]. The algorithm is the same as the AM algorithm except when a candidate is rejected (first step of DR) the other candidate is generated with respect to scaled covariance matrix. In other words, on first step of DR candidate $\hat{\theta}^{(1)}$ is generated from proposal distribution $q_1(\cdot, \theta_n|\mathbf{C}_n^1)$, on the other steps the candidates $\hat{\theta}^{(i)}$ is generated from $q_i(\cdot, \hat{\theta}^{(i-1)}, ..., \hat{\theta}^{(1)}, \theta_n|\mathbf{C}_n^i)$, where $\mathbf{C}_n^i = \gamma_i \mathbf{C}_n^1$. γ_i is an scaling parameter that can be chosen freely. The basic flowchart of the DRAM algorithm is presented on fig. 9.

In this thesis, MCMC Toolbox for MATLAB written by Marko Laine was used in order to implement the DRAM algorithm. The code and the examples can be seen at `https://mjlaine.github.io/mcmcstat/`. This package allows using MH and AM algorithms as well.

The data used in this work consists of several (11) time series that represent estimates of historical yearly global temperatures (for more details see the next Section). The mean value of these estimates is used as the 'measurement'. No rigorous statistics is available for it, but an i.i.d. Gaussian distribution assumption was considered reasonable, even if the mean is taken over 11 values only. A key issue is how to estimate the scalar variance of the Gaussian likelihood. Two options were considered: estimate the variance of the mean directly from the replicate data, or estimate it by the residuals of the MCMC fits during the parameter sampling. The latter can be done by the MCMC toolbox using the so called conjugate prior sampling. It turned out that both approaches lead practically to the same results. This can be taken as a confirmation that the model fit (i.e., the residu-

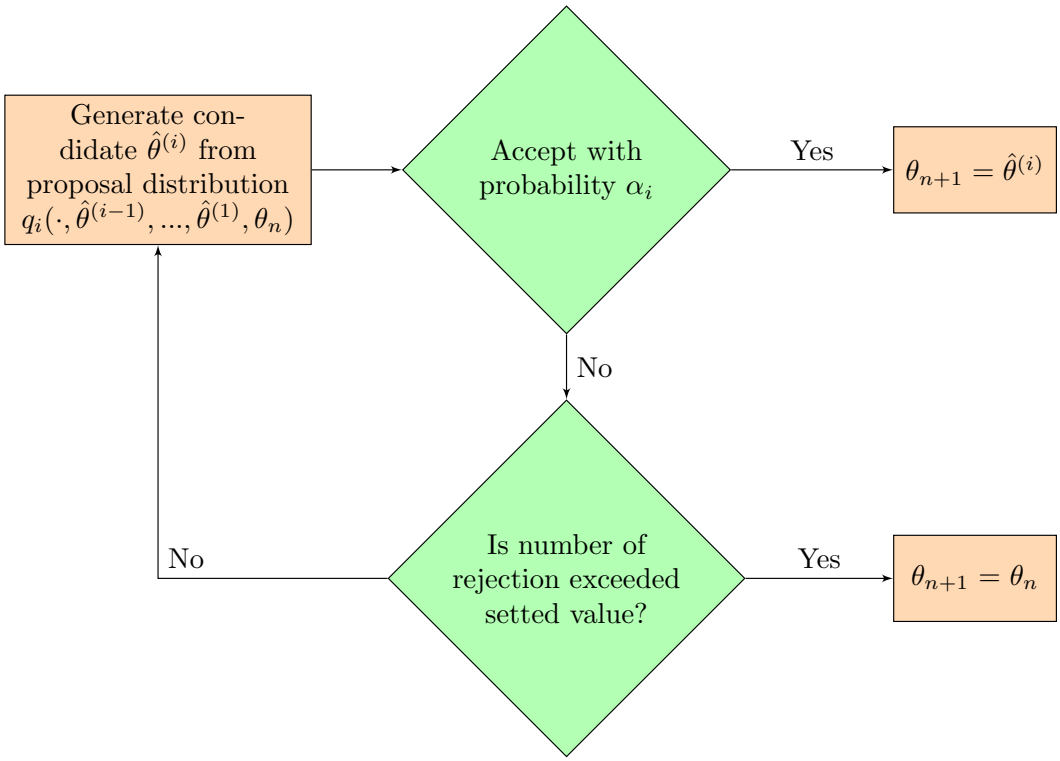

Figure 8. Generating and acceptance in Delayed Rejection algorithm. n is the length of the chain, i is the number of generated candidates

als) via MCMC sampling agrees with the level of uncertainty available for the historical temperature time series.

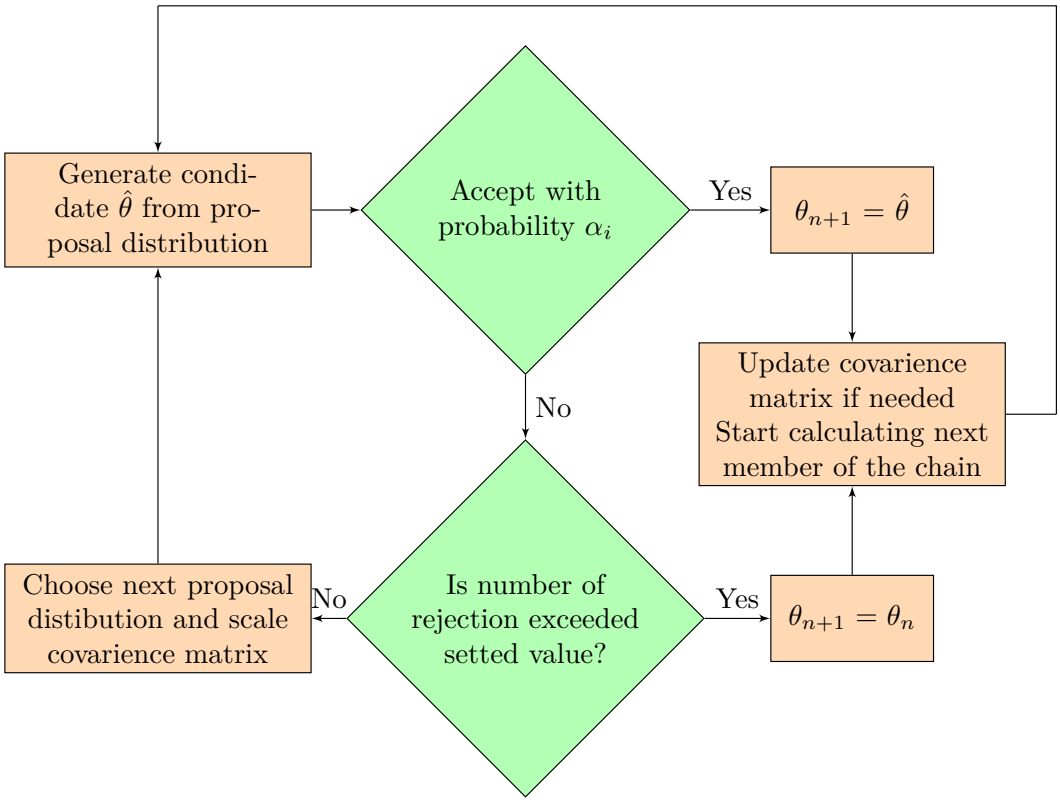

Figure 9. Delayed Rejection Adaptive Metropolis algorithm

3 EXPERIMENTS

This Section presents description of the experiments, set of parameters and temperature dataset that were used, and the results.

3.1 Chosen parameters

As was mentioned above, a simple sensitivity analysis was conducted in the paper by Smith et al. [8] by using Monte Carlo simulation and the set of 21 prior distributions of FaIR's parameters. Nevertheless, the set of 20 parameters were used in this work since forcing due to doubling of CO_2 $F_{2\times}$ directly depends on the scaling factor F_0. $F_{2\times}$ is set to $3.71 \times F_0$ which corresponds to the default FaIR value. In the others respects, the set is fully identical to the set used by Smith et al. The set, names of parameters, and their priors are presented in table 3.

The parameters can be devided into three types based on the part of the FaIR calculation where they are used (calculation of concentration, ERF, and temperature). r_0, r_{C}, r_{T} are used in the calculation of CO_2 concentration (eq. (2)). TCR, ECS, d_1, d_2 are responsible for calculation of temperature change caused by radiative forcing (eqs. (21) and (22)). $F_i;\ i = 0, ..., 12$ are scaling factors of all 13 forcing groups (Section 2.1.2, see table 4 for correspondence of F_i to the forcing groups).

The parameters of the set allow tuning almost all aspects of the model (calculation of CO_2 concentration, scaling of all 13 forcing groups, and temperature calculation) and at the same time avoiding an enormous number of sampled parameters what can potentially lead to an increase of the convergence time. A sensible extension of the set would be the substitution of the scaling parameter F_3 by the scaling factors for all 27 ERFs of the "Other GHG", but it greatly increases the size of the set.

As shown in table 3, most of the parameters have priors with a normal or log-normal distribution that are no need to define. The other, not straightforward distributions, are described below.

All variables are considered to be independent of each other except TCR and ECS, which have a strong correlation. Their prior is a log-normal joint distribution with parameters calculated from the data from Forster et al. [2] (as in the Smith et al. [8]). The probability

Table 3. Set of control variables used for MCMC chain calculation and their priors distributions. In cases of Log-Normal distributions means and standard deviations of logarithmic values are indicated

Index	Parameter	Prior Distribution	Parameters of the prior distributions
1	r_0	Normal	Mean: 35 StD: 2.77
2	r_C	Normal	Mean: 0.019 StD: 0.0015
3	r_T	Normal	Mean: 4.165 StD: 0.33
4	TCR	Log-Normal	$\boldsymbol{\mu} = \begin{pmatrix} 0.58 \\ 1.14 \end{pmatrix}; \boldsymbol{\Sigma} = \begin{pmatrix} 0.048 & 0.045 \\ 0.045 & 0.062 \end{pmatrix}$
5	ECS	Log-Normal	
6	d_1	Normal	Mean: 239 StD: 63
7	d_2	Normal	Mean: 4.1 StD: 1
8	F_0	Normal	Mean: 1 StD: 0.12
9	F_1	Normal	Mean: 1 StD: 0.17
10	F_2	Normal	Mean: 1 StD: 0.12
11	F_3	Normal	Mean: 1 StD: 0.12
12	F_4	Normal	Mean: 1 StD: 0.30
13	F_5	Normal	Mean: 1 StD: 1.26
14	F_6	Normal	Mean: 1 StD: 0.44
15	F_7	Log-Normal	Mean: 0 StD: 0.65
16	F_8	Two Half-Normal	$\mu = 1$ $\sigma_1 = 0.56;\ \sigma_2 = 0.66$
17	F_9	Log-Normal	Mean: 0 StD: 0.50
18	F_{10}	Normal	Mean: 1 StD: 1.01
19	F_{11}	Normal	Mean: 1 StD: 0.30
20	F_{12}	Normal	Mean: 1 StD: 0.14

Table 4. Indexes of scaling parameters F_i and their respective radiative forcing groups

i	Agent	i	Agent
0	CO_2	7	Contrails
1	CH_4	8	Aerosols
2	N_2O	9	Black carbon on snow
3	Other GHG	10	Land use change
4	Tropospheric ozone	11	Volcanic
5	Stratospheric ozone	12	Solar
6	Stratospheric water vapour		

density function is

$$P(\boldsymbol{x}) = \frac{1}{2\pi\sqrt{\det \boldsymbol{\Sigma}}} \prod_{j=1}^{2} \left(x_j^{-1}\right) \exp\left(-\frac{1}{2}(\ln(\boldsymbol{x}) - \boldsymbol{\mu})^{\mathrm{T}} \boldsymbol{\Sigma}^{-1} (\ln(\boldsymbol{x}) - \boldsymbol{\mu})\right) \tag{31}$$

where $\boldsymbol{\mu}$ - mean vector of logarithmic values and $\boldsymbol{\Sigma}$ - covariance matrix of logarithmic values.

Prior of the aerosol scaling factor is two half-normal distribution and has probability density function

$$P(x) = \sqrt{\frac{2}{\pi}} \frac{1}{(\sigma_1 + \sigma_2)} \exp\left(-\frac{1}{2}\left(\frac{x-\mu}{\sigma_i}\right)^2\right), \tag{32}$$

$$\text{where } \sigma_i = \begin{cases} \sigma_1, & \text{if } x \leq \mu \\ \sigma_2, & \text{if } x > \mu \end{cases}, \tag{33}$$

μ is the mode and σ_i are StD of normal distributions from half of which two half-normal distribution is constructed.

The initial points of the MCMC are the same values as default FaIR parameters: for r_0, r_{C}, r_{T}, d_1, d_2 – the mean values, for TCR and ECS – 1.6 K and 2.75 K respectively, and for F_i the initial points are equal to 1.

3.2 Temperature dataset

In this work, a temperature dataset was used as an observed measurements. It consists of temperature output of 11 different climate models during the historical experiment where atmospheric composition, emissions or concentrations of short-lived agents, solar forcing, and land use are imposed to correspond to observations (see [9] for details).

The dataset was collected by the scientists from GCESS Beijing Normal University and processed and provided to us by the XDC Model Team from right. based on science GmbH. Processing consisted of calculation of annual average temperature for each model and leveling of outputs by substructure average of temperature during 1850-1899.

The dataset and the mean annual value are depicted on fig. 10.

Mean annual temperature was used as an observed measurement. The mean annual variance divided by the number of measurements (11) was used as measurement error variance (see Section 2.3 for details). The test runs of the MCMC toolbox showed that there was not any significant difference in the estimation of the parameters between cases when conjugate prior sampling for the error variance was employed, or when the error variance was fixed directly by repeated data. Therefore, the chains presented below are calculated without error update.

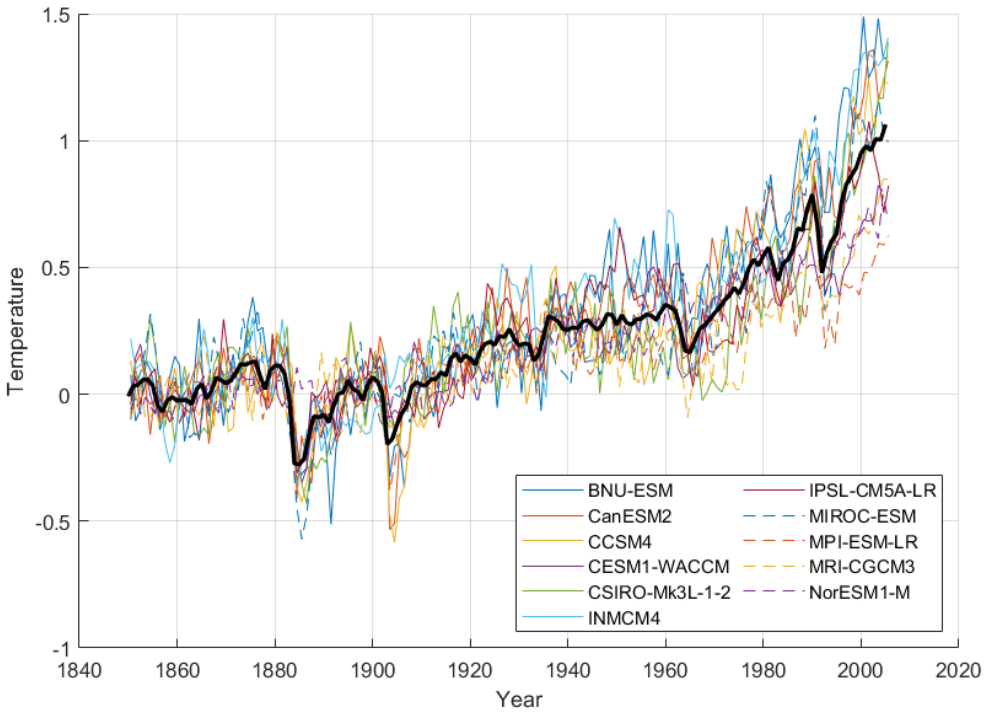

Figure 10. Temperature dataset. The black line is the mean annual values that was treated as observed measurements

3.3 Description of the experiments

Three chains were calculated with the same set of control parameters but with different priors. They can be consequentially called: "without priors", "with priors" and "with bounds".

In the first experiment priors are uniform and most of them are without limits. That means that this parameters are not restricted and can take any value. Exceptions are parameters r_0, r_{T}, r_{C}, F_0, F_2, F_3 which are restricted to positive values and $\mathrm{TCR} \in [1, 3]$, $\mathrm{ECS} \in [1, 6]$, $d_1 \in [50, 428]$, $d_2 \in [1.1, 7.1]$. This restriction exist to avoid overflow during calculation.

In the second experiment, the parameters have priors that were described in Section 3.1 and correspond to priors that were used in the article by Smith et al. [8].

In the third experiment priors are uniform but with limits that correspond to $\mu \pm 3\sigma$ values from priors from the second experiment. TCR and ECS are exceptions that have bounds at $[1.05, 2.41]$ for TCR and $[2.01, 4.22]$ for ECS, which are $5 - 95\%$ credible intervals according to [8]. In other words, parameters can take any values that lay inside of the interval corresponding to physically possible values.

3.4 Outcome of the experiments

As was mentioned above, three chains with various groups of priors were calculated. The sum of squares (SS) values of the chains can be seen on fig. 11. The SS values of all three chains undergo a sharp decrease at the start from 0.519 (what correspond to the default FaIR parameters) to 0.25 and bellow. The second and the third chains ("with priors" and "with bounds" respectively) rapidly become stable in the terms of SS values, when the same takes almost $100,000$ steps for the first ("without priors") chain.

All chains were generated until a sufficient sample size of the posterior distribution is achieved. There is no strict rule about acceptable chain length, however, chains of length $250,000$ (first chain) and $100,000$ (second and third) were calculated. In our opinion, those lengths provide enough sample size (with respect to a 'stable' state in terms of SS values) to work with.

Hereinafter, when discussing the results we refer to the second part of the chains (when

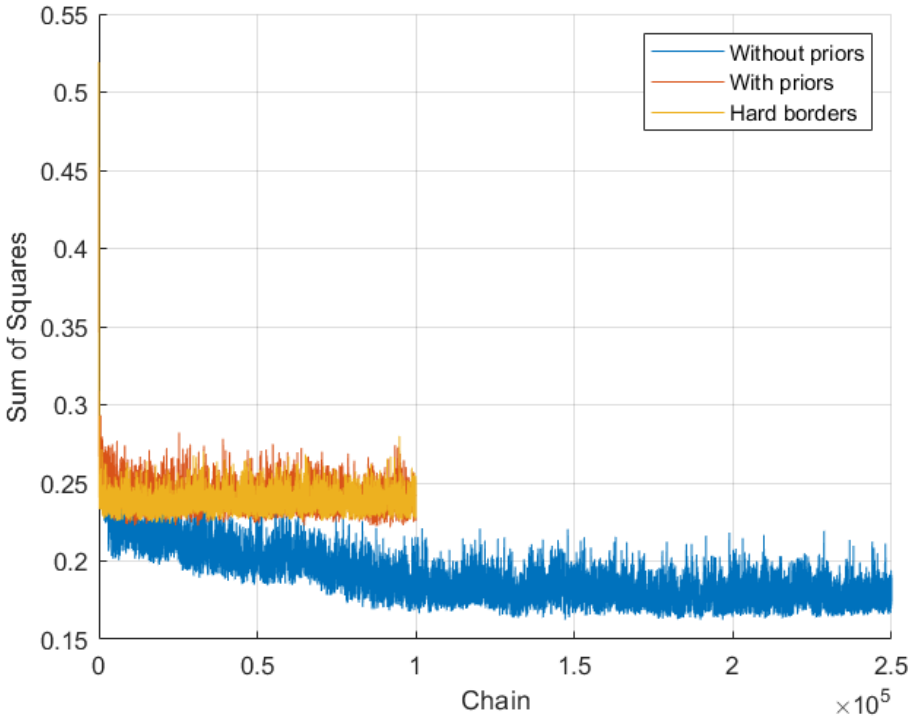

Figure 11. Sum of Squares values for the chains

they are in a stable state) since at the start the sequence must progress from the initial point to the stable state where the sampling of the posterior distribution is occurring. The statistics of the second part of the chains are shown in table 5. Histograms of the second parts of the chains can be seen in appendix 1.

Table 5. Statistic of Sum of Square values of the chains depicted on fig. 11. Only second half of the chain was is considered

Name of chain	Mean	5% quantile	95% quantile
Without priors	0.179	0.168	0.191
With priors	0.240	0.230	0.253
With bounds	0.237	0.230	0.248

Although, the first ("without priors") chain has smaller SS values and hence shows better fit results than the others, these results can not be used for uncertainty estimation since, in that case, the parameters take values out of the acceptable range defined by priors from Smith et al.

In order to discuss the results and present some representative posterior distributions and chains' behaviour three examples are presented below. Here, as well as in appendix 1,

blue lines indicate prior distribution described in Smith et al [8].

Figure 12 shows an example of different postrior distribution of parameter r_{C} in all three experiments. In the first experiment ("without priors") mean value and variance of the sampled posterior distribution (indicated by histogram) are much bigger than the prior one. In contrast, in the second experiment ("with priors"), the posterior distribution is very close to the prior. Finally, in the third experiment ("with bounds"), the chain has a distribution similar to a uniform one. As the result, the small influence of the parameter r_{C} on the quality of the fit can be concluded. In addition, that example shows the reason why the first chain can not be used in uncertainty evaluation: parameter r_{C} takes values much higher than the prior.

(a) Without Priors

(b) With Priors

(c) Bounds

Figure 12. Comparison of the results of MCMC for the parameter r_{C}. The histograms represent the second half of the chain and blue lines represent prior from Smith et al.

As an example of the different parameter's posterior distributions in the same chain, F_6 and F_8 during the second experiment ("with priors") are presented on fig. 13. F_6 has the posterior distribution close to the prior one, while the distribution of F_8 has a much smaller variance, showing improvement in the parameter estimation compare to the prior.

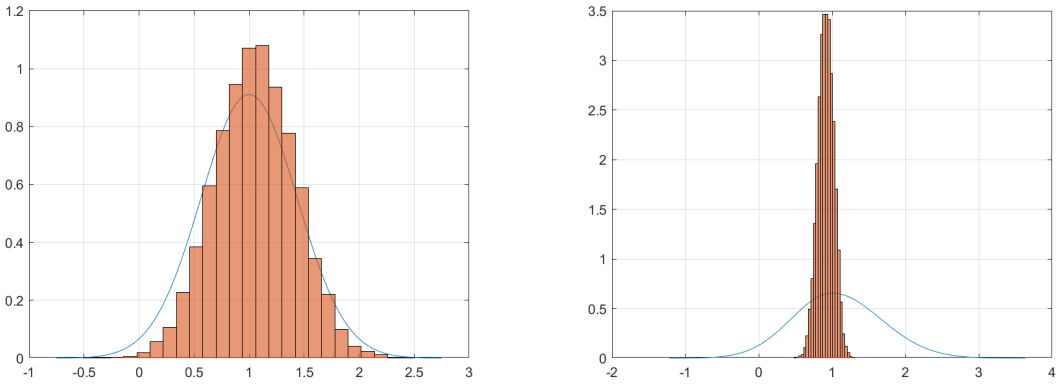

(a) F_6 (b) F_8

Figure 13. Comparison of the "with priors" chain. Parameters F_6 (Stratospheric water vapour) and F_8 (Aerosols). The histograms represent the second half of the chain and blue lines represent prior from Smith et al.

Finally, the third example is a comparison of the postrior distribution of TCR and ECS (that have log-normal joint prior distribution) among all three chains (fig. 14). Here, the red dashed lines indicate the prior. During the first experiment, the chain's distribution is broad and the maximum lays far from the prior. The second experiment, however, shows better results with small variance and maximum laying inside of the possible area. The results of the third experiment have a higher variance than in the second one but lower than in the first one. Nonetheless, the maximum of the distribution is close to the maximum of the second chain.

Looking ahead, it worth noticing that the FaIR model simulates the rapid temperature drops, which can be seen on fig. 10. Furthermore, the reason for the drops can be clearly seen in input data or, more precisely, in volcanic radiative forcing time-series. Figure 15 shows volcanic RF against historical temperature (see Section 3.2). It is clear that all major temperature drops correspond with increases of negative radiative forcing caused by volcanic eruptions.

FaIR uses GHG emissions and volcanic and solar RF time-series in order to calculate concentrations, ERFs (of the others 11 groups), and, finally, temperature. In order to calculate temperature and discuss the uncertainties of the model, default RF time-series that are integrated into FaIR model and two different emission time-series: RCP 8.5 and XDC, were used.

Representative Concentration Pathways or RCP are a set of four pathways designed as representative scenarios for climate modelling. All four scenarios are in the FaIR tool-

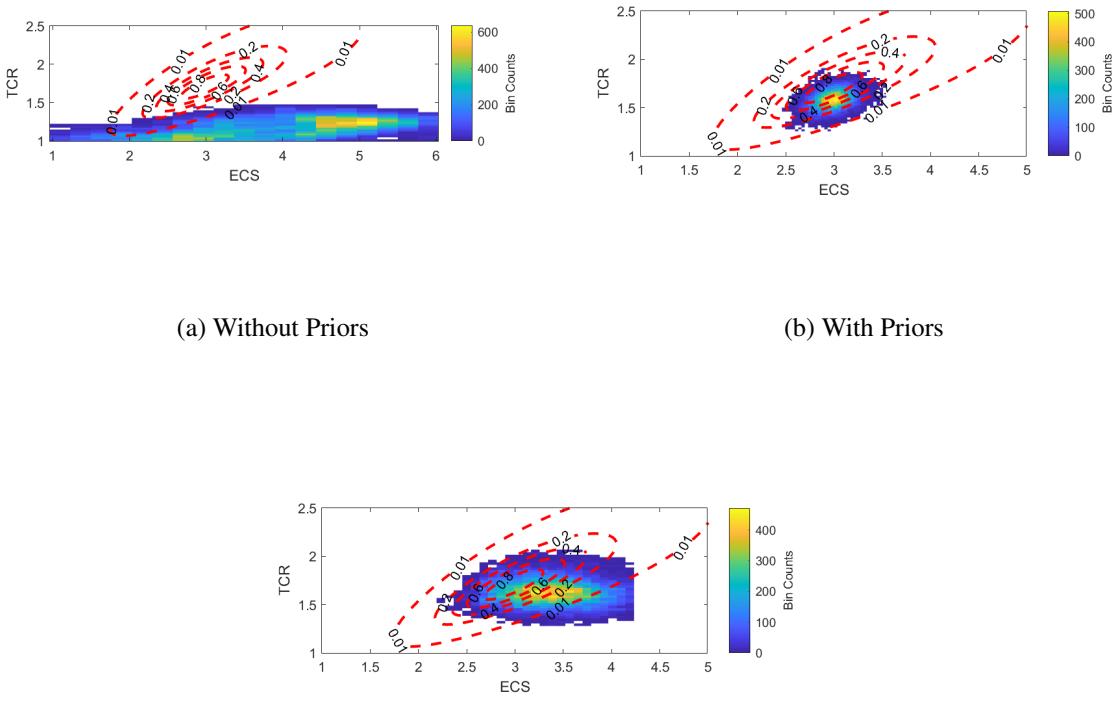

(a) Without Priors

(b) With Priors

(c) Without Bounds

Figure 14. Comparison of the chains for the parameters TCR and ECS. The red dashed lines correspond to the prior from Smith et al.

box. RCP 8.5 is the most emission-heavy scenario in the set and corresponds to the case when radiative forcing is equal to $8.5\,\mathrm{W\,m^{-2}}$ by the year 2100. For more details see Vuuren et al. [11].

By XDC emission we mean an example XDC emission scenario calculated according to Section 2.2 for a company from the chemical industry. The example was provided to us by the XDC Model Team from the right. based on science GmbH. The calculated CO_2 emission replacing the same emission in the RCP 8.5 pathway. In other words, the XDC emission scenario is the same as the RCP 8.5 scenario except for CO_2 fossil emission. Figure 16 shows this difference. XDC emission is undergoing a sharp increase in the year 2017, which corresponds to the base year or, in the other words, when "all economical entities start to operate with the same emission intensity as the one under consideration".

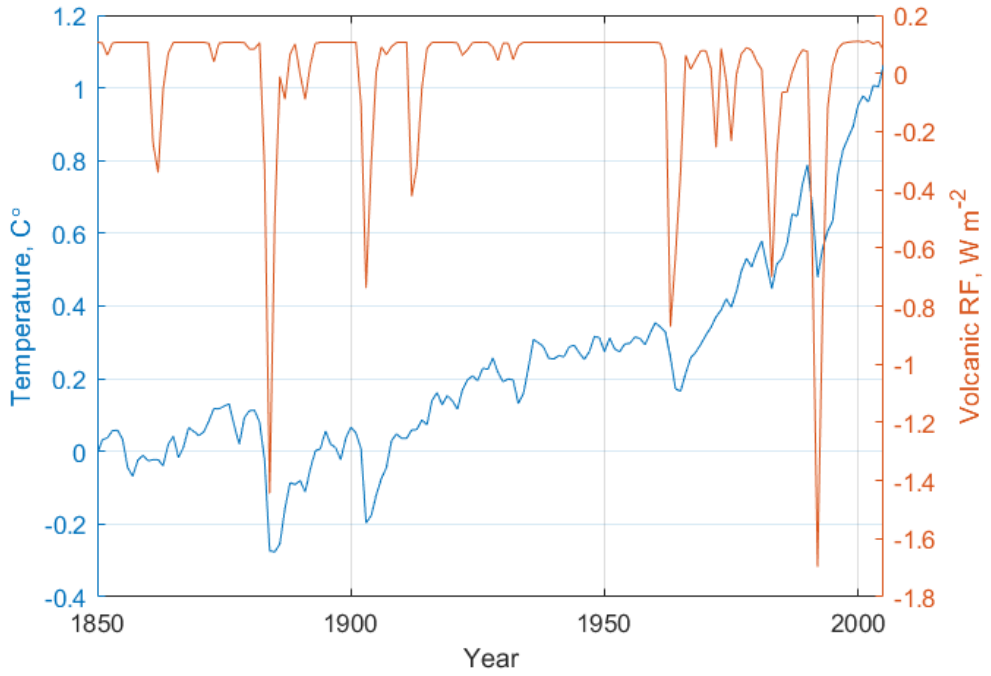

Figure 15. Historical temperature and volcanic radiative forcing

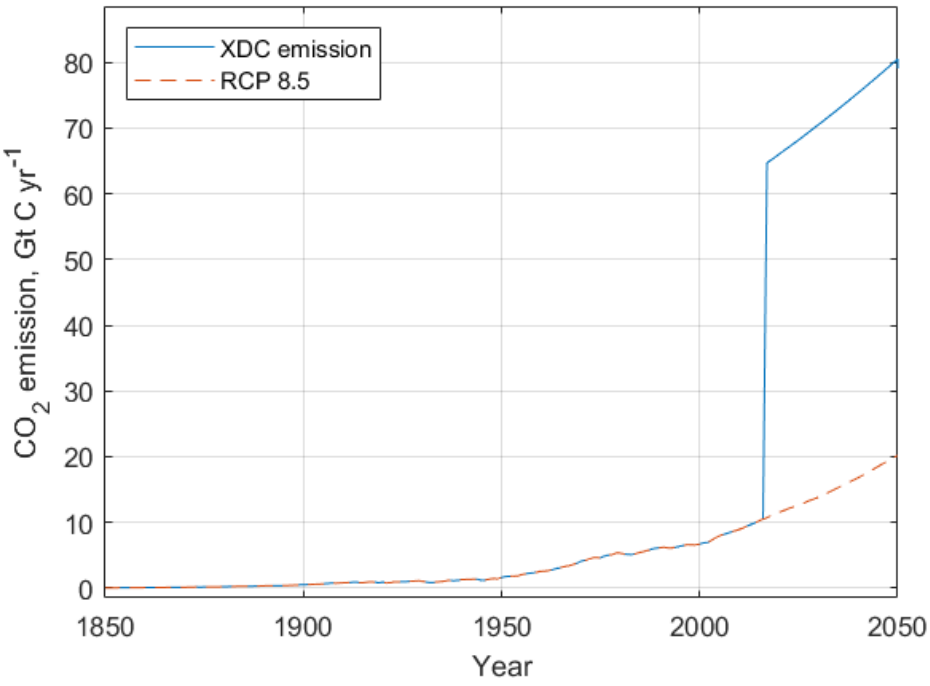

Figure 16. Comparison of XDC and RCP 8.5 CO_2 emission

3.4.1 RCP 8.5 emission scenario

Here we will discuss the uncertainties of FaIR temperature calculation. The results presented in this subsection are calculated with the RCP 8.5 emission scenario. Furthermore, since the sampled posterior distribution of the first experiment ("without priors") can not be used for uncertainness estimation, only cases with second and third chains are taken into the account.

Figures 17 and 18 show overall fit and prediction of the FaIR model. Solid lines indicate the median value and the area around them correspond to 5-95% certain intervals. The crosses represents the historical temperature dataset (see Section 3.2). Red line and filled area correspond to the second experiment ("with priors") and the blue ones – to the third ("with bounds")

Figure 17 depicts the time period 1850-2005 that the temperature dataset covers. This graph shows the quality of the fit. As can be seen, the modeled temperatures fit the data moderately sufficient, especially after 1950, and have the same drops that are most likely caused by volcanic activities.

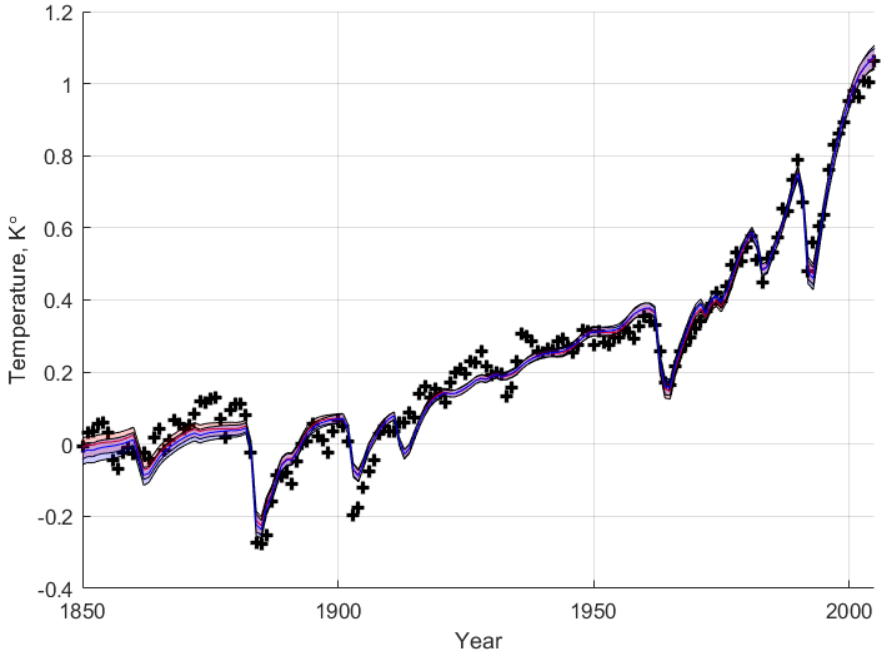

Figure 17. Median temperatures and their uncertainties based on "with priors" (red) and "with bounds" (blue) chains. Black crosses – historical data. RCP 8.5 scenario. 1850-2005

Figure 18 shows the prediction part: the time period 2000-2050. The median temperatures are close to each other and located inside of each other's confidence interval. The uncertainties are also increasing with time after the end of the temperature dataset (2005). The median and the 5-95% quantiles by the year 2050 are: $2.433\,(2.258,\ 2.614)$ for the second chain ("with priors"); $2.505\,(2.278,\ 2.737)$ for the third chain ("with bounds").

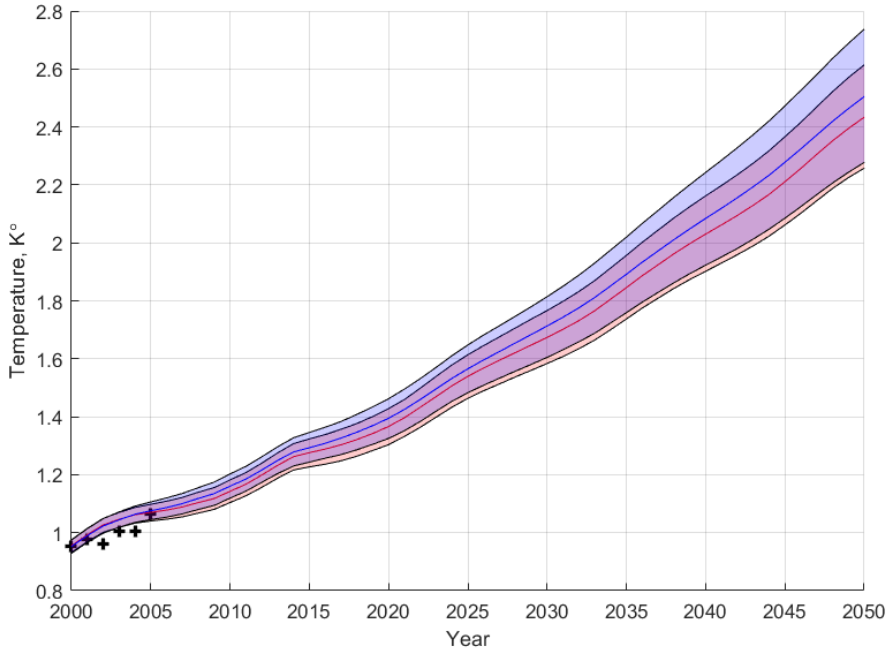

Figure 18. Median temperatures and their uncertainties based on "with priors" (red) and "with bounds" (blue) chains. Black crosses – historical data. RCP 8.5 scenario. 2000-2050

In order to validate the decrease of temperature uncertainty, a simple Monte-Carlo simulation was conducted. All 20 parameters were randomly generated according to their priors from Smith et al. 1000 times and the FaIR model was run with that parameters. The results are shown in fig. 19. It is clear that overall uncertainty is higher during fit and prediction periods. By the year 2050 median and 5-95% quantiles are $2.5567\,(1.551,\ 3.971)$. When the median temperature is relatively close to the median temperature calculated from posterior distributions, the uncertainties interval is much wider ($2.42\,\mathrm{C}^\circ$ against $0.356\,\mathrm{C}^\circ$ and $0.459\,\mathrm{C}^\circ$). This shows a significant improvement of uncertainty estimation by using a posterior distribution with sensitivity analysis compare to prior distribution with Monte-Carlo simulation.

Worth to notice that the Monte-Carlo simulation results, strictly speaking, do not correspond to the results presented in the Smith et al. [8] since in the authors used more restrictions for the parameters, for example, strict limits for parameters d_1 and d_2, as well

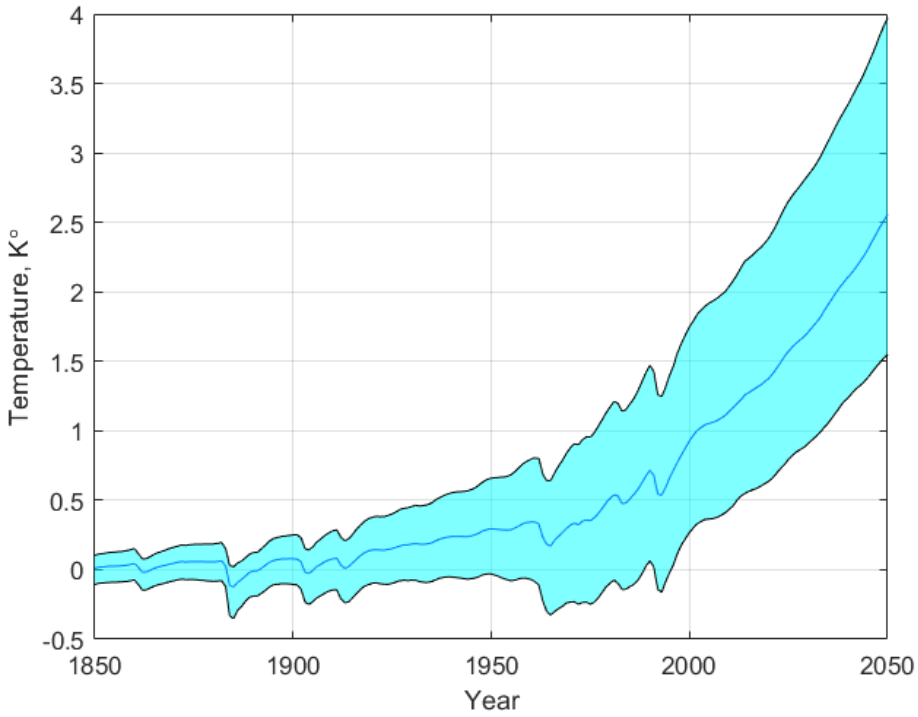

Figure 19. Monte Carlo simulation with priors from Smith et al. 90% certainty interval

as the fact that in the paper set of 21 parameters were used. Nonetheless, even comparing results calculated from postrior with the ones presented by Smith, the uncertainty is significantly smaller, however that can be partially be caused by the reduced number of controlled parameters.

At last, fig. 20 depicts calculated CO_2 concentration. The concentration in both cases increases with acceleration and since the CO_2 emission (see fig. 16) does not undergo rapid changes the concentration also does not have any spikes.

3.4.2 XDC emission scenario

In this part, the results calculated by using the XDC emission scenario are presented and discussed. As for the RCP 8.5, only posterior distributions sampled by the second ("with priors") and the third ("with bounds") chains are taken into consideration.

Figures 21 and 22 show the temperature calculation with the same notation as in Section 3.4.1.

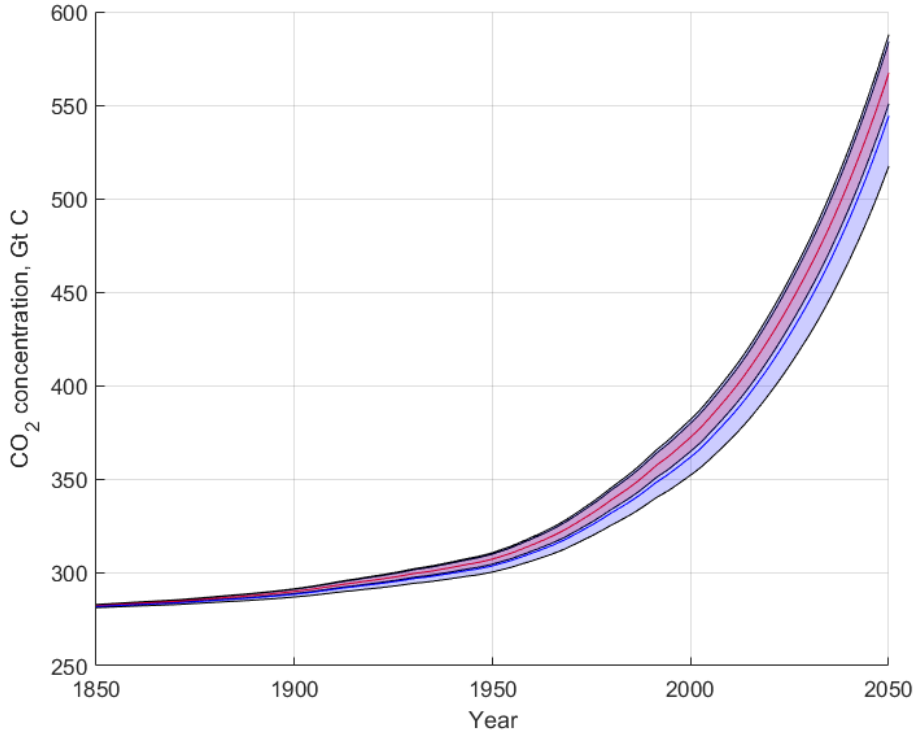

Figure 20. Concentration of CO_2. RCP 8.5 scenario. Red - "with priors"; Blue - "with bounds"

Figure 21 depicts time period of 1850-2005. The results are essentially the same as on fig. 17 what was expected. As was described in Section 2.1, the FaIR model sequentially calculates temperature from the previous year to the next one. Since all input data is the same until the year 2017 (see fig. 16), the modeling results are the same until the change in the input data.

Therefore, in the prediction part (2000-2050) that is shown in fig. 22 the results significantly differ from the RCP 8.5 scenario. The temperature increase becomes quicker after the year 2017 and, as a result, median temperatures are much higher than the ones in the RCP 8.5 emission scenario case. The median and 5-95% quantiles by the year 2050 are 4.319 (3.794; 4.927) for the second chain ("with priors") and 4.603 (3.892; 5.409) for the third chain ("with bounds"). The uncertainty intervals are also higher than previously, $1.133\,\mathrm{C}^\circ$ against $0.356\,\mathrm{C}^\circ$ for the second chain and $1.517\,\mathrm{C}^\circ$ against $0.459\,\mathrm{C}^\circ$ for the third chain.

The CO_2 concentration, depicted on fig. 23, is also undergoing rapid change after 2017.

Overall, the results are expected. The increase of CO_2 emission causes the increase of the CO_2 concentration what is the cause of CO_2 ERF increase, what cases the temperature

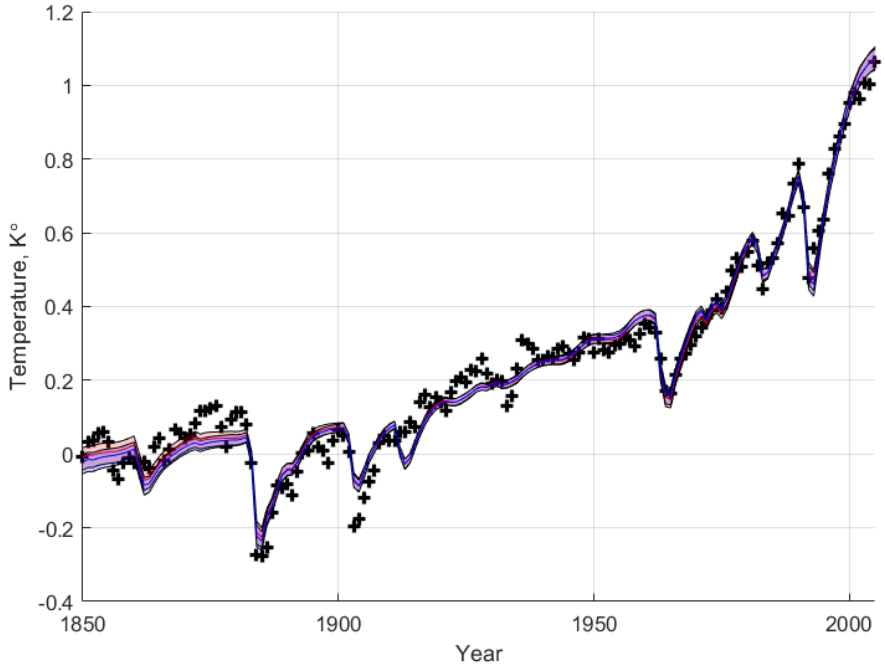

Figure 21. Median temperatures and their uncertainties based on "with priors" (red) and "with bounds" (blue) chains. Black crosses – historical data. XDC. 1850-2005

increase. Nonetheless, it is important to see that the FaIR model and uncertainty estimation can work with this type of input emission and the solution does not diverge and hence the results of this thesis can be used for the XDC model. It also can be considered to be expected since the main motivation behind the FaIR design was the creation of a simple climate model that can more precise calculate cases with impulse emission.

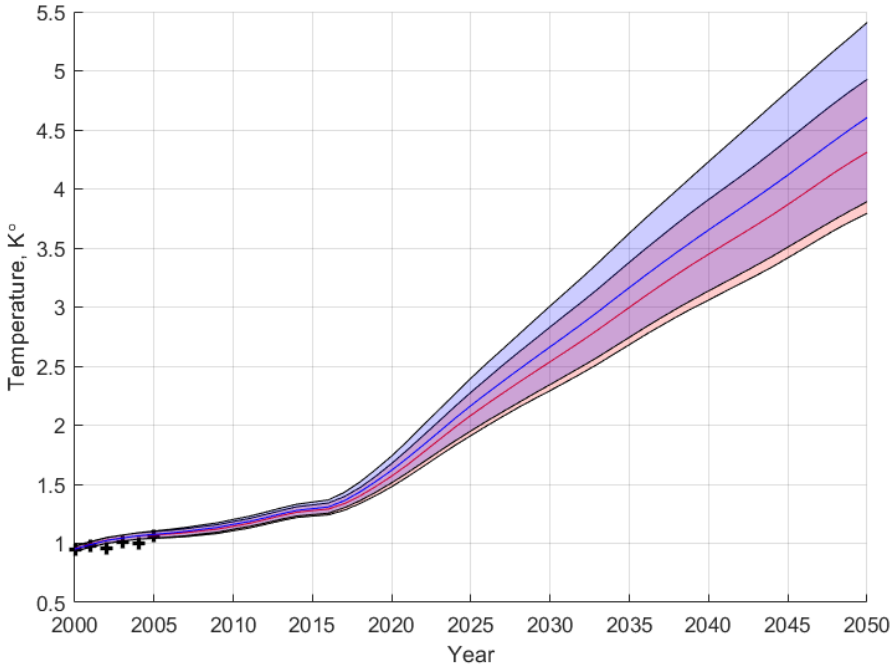

Figure 22. Median temperatures and their uncertainties based on "with priors" (red) and "with bounds" (blue) chains. Black crosses – historical data. XDC. 2000-2050

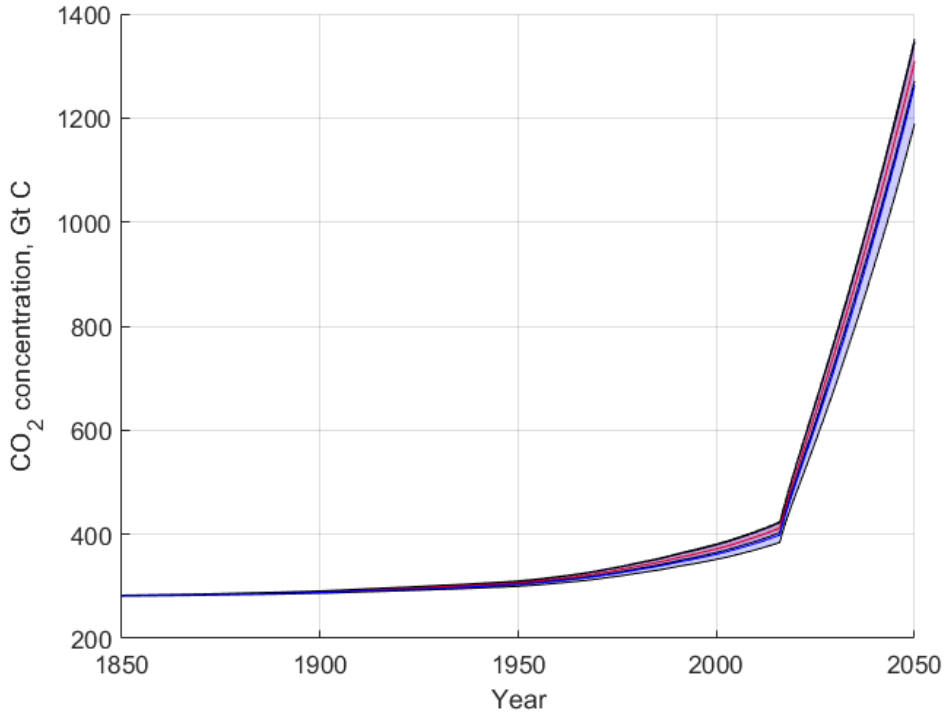

Figure 23. Concentration of CO_2. XDC scenario. Red - "with priors"; Blue - "with bounds"

4 DISCUSSION

The research goal of this thesis was to conduct sensitivity analysis of the FaIR model by using Markov chains Monte Carlo and the historical temperature dataset that is consists of processed outputs of 11 different climate models during the "historcial" CMIP5 experiment.

Three chains were calculated to sample posterior distributions of the 20 parameters. Differences between these three experiments were the different sets of the priors: without priors, with priors from the paper by Smith et al. [8], and, finally, with uniform priors with limits that correspond to the priors from Smith et al.

While the first chain can not be used in order to estimate the FaIR uncertainties since the parameters take values outside of the possible range, the second and the third chains allow evaluating the model's error. The results show that by using posterior distribution the uncertainties of the model are significantly smaller compare to the results obtained by the direct Monte-Carlo simulation given priors of the parameters.

In addition, it was shown that the findings of the thesis can be also used for the X-Degree Compatibility model. XDC model is an economic climate impact model that is used for the estimation of climate change caused by an economical entity. It calculates a hypothetical CO_2 emission that depends on the entity's GHG emission and uses it as input for the FaIR model. This hypothetical emission can have rapid changes and, therefore, it was important to verify that this type of input does not lead to divergence of the solutions.

Compare to the uncertainty quantification that was conducted in Smith et al. [8], where a simple Monte-Carlo simulation by sampling FaIR's parameters directly from their priors (with some limitations) was used, the results of this work shows better results in terms of the fit of the data (see Section 3.2 for details about the data) and lower errors uncertainty. therefore, it was important to verify that this type of the input does not leads to divergence of the solutions.

The framework of the thesis has few delimitations and, therefore, several ways to continue the work exists.

First of all, the investigation of the other sources of uncertainties. In this work the influence of the set of the 20 internal FaIR parameters was excitement. Nonetheless, several other sources of error exist. The most obvious ones are the input time-series such as the

greenhouse gas emissions and solar and volcanic radiative forcing.

Secondly, adding the other outputs of the FaIR model under consideration of the quality of the fit. FaIR's output consists of temperature, concentration, and effective radiative forcing time-series. The addition of the others outputs to the metric of the quality of the fit can be beneficial to narrow the posterior distribution of the parameters even more.

REFERENCES

[1] Maryam Etminan et al. “Radiative forcing of carbon dioxide, methane, and nitrous oxide: A significant revision of the methane radiative forcing”. In: *Geophysical Research Letters* 43.24 (2016), pp. 12–614.

[2] Piers M Forster et al. “Evaluating adjusted forcing and model spread for historical and future scenarios in the CMIP5 generation of climate models”. In: *Journal of Geophysical Research: Atmospheres* 118.3 (2013), pp. 1139–1150.

[3] Heikki Haario, Eero Saksman, Johanna Tamminen, et al. “An adaptive Metropolis algorithm”. In: *Bernoulli* 7.2 (2001), pp. 223–242.

[4] Heikki Haario et al. “DRAM: efficient adaptive MCMC”. In: *Statistics and computing* 16.4 (2006), pp. 339–354.

[5] H Damon Matthews et al. “The proportionality of global warming to cumulative carbon emissions”. In: *Nature* 459.7248 (2009), pp. 829–832.

[6] Richard J Millar et al. “A modified impulse-response representation of the global near-surface air temperature and atmospheric concentration response to carbon dioxide emissions”. In: *Atmospheric Chemistry and Physics* 17.11 (2017), pp. 7213–7228.

[7] G. Myhre et al. “Anthropogenic and Natural Radiative Forcing”. In: *Climate Change 2013 – The Physical Science Basis: Working Group I Contribution to the Fifth Assessment Report of the Intergovernmental Panel on Climate Change*. Ed. by Daniel Jacob, A.R. Ravishankara, and Keith Shine. Cambridge University Press, 2014. Chap. 8, pp. 659–740. DOI: 10.1017/CBO9781107415324.018.

[8] Christopher J Smith et al. “FAIR v1. 3: a simple emissions-based impulse response and carbon cycle model”. In: *Geoscientific Model Development* 11.6 (2018), pp. 2273–2297.

[9] Karl E Taylor. “A summary of the CMIP5 experiment design”. In: *http://cmip-pcmdi. llnl. gov/cmip5/docs/Taylor_CMIP5_design. pdf* (2009).

[10] Luke Tierney. “Markov chains for exploring posterior distributions”. In: *the Annals of Statistics* (1994), pp. 1701–1728.

[11] Detlef P Van Vuuren et al. “The representative concentration pathways: an overview”. In: *Climatic change* 109.1 (2011), pp. 5–31.

Appendix 1. Sampled posterior distribution

1.1 Results from the 1st experiment ("Without priors").

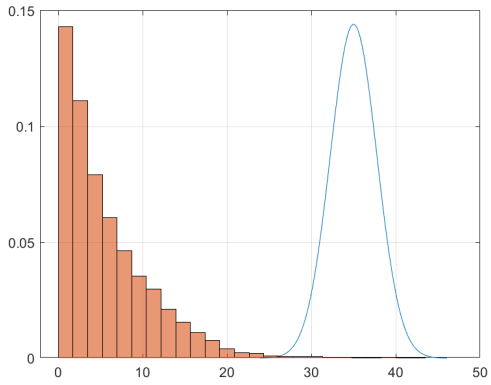

(a) r_0

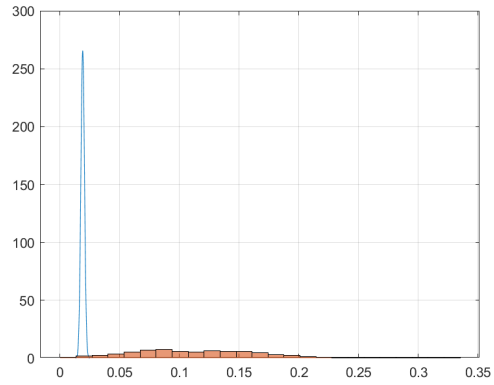

(b) r_C

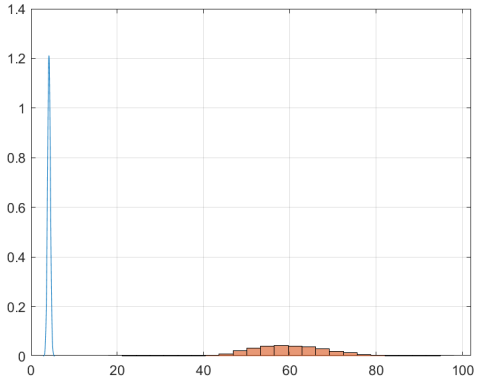

(c) r_T

Figure A1.1. Sampled posterior distribution of parameters responsible for CO_2 concentration calculation. "Without priors" chain. Blue line corresponds to the the prior distribution from Smith et al. [8].

(continues)

Appendix 1. (continued)

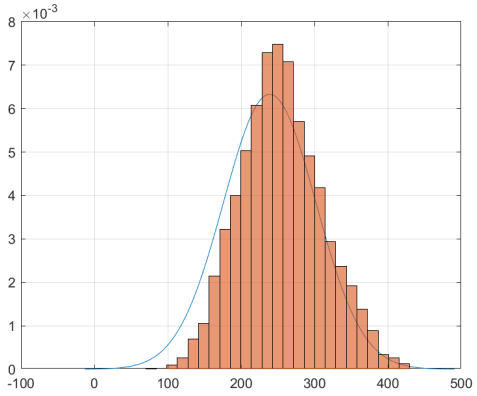

(a) d_1

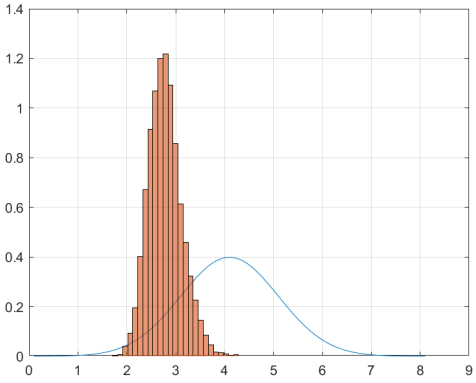

(b) d_2

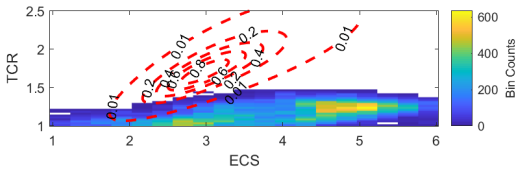

(c) TCR and ECS

Figure A1.2. Sampled posterior distribution of parameters responsible for temperature calculation. "Without priors" chain. Blue line corresponds to the the prior distribution from Smith et al. [8].

(continues)

Appendix 1. (continued)

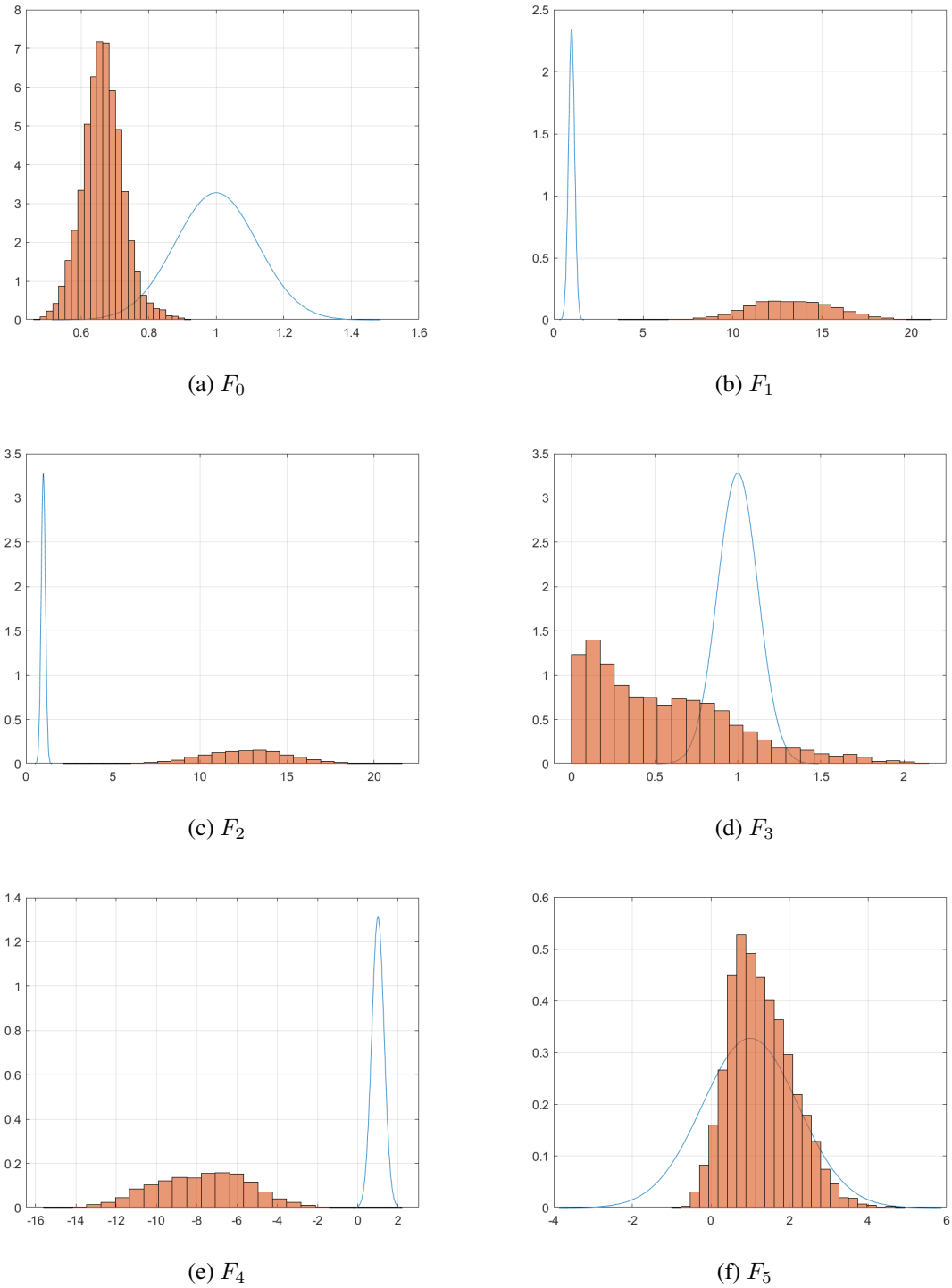

(a) F_0 (b) F_1

(c) F_2 (d) F_3

(e) F_4 (f) F_5

Figure A1.3. Sampled posterior distribution of scaling parameters of forcing groups with indexes from 0 to 5. "Without priors" chain. Blue line corresponds to the the prior distribution from Smith et al. [8].

(continues)

Appendix 1. (continued)

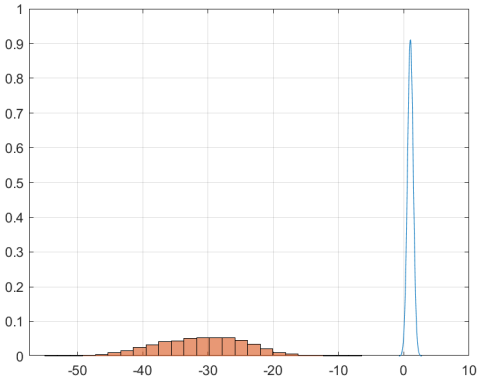

(a) F_6

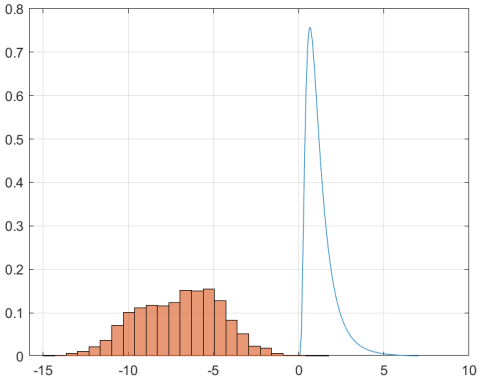

(b) F_7

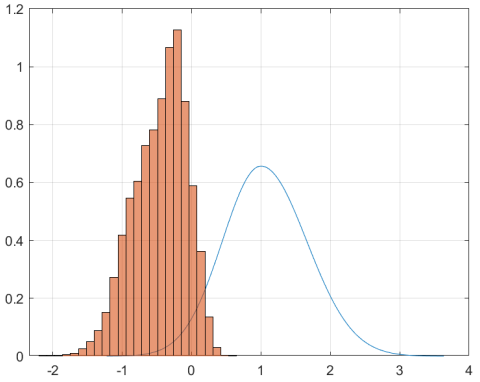

(c) F_8

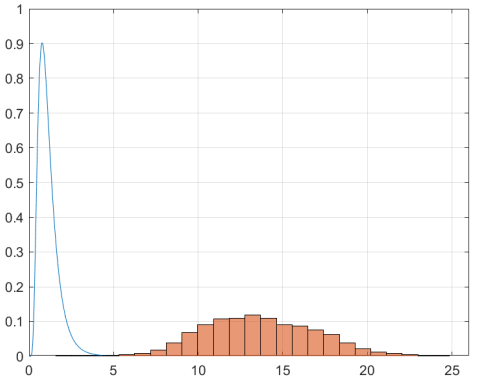

(d) F_9

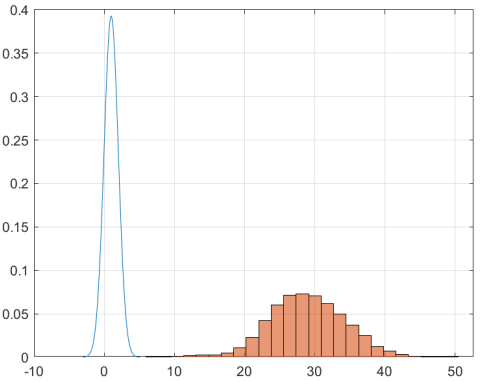

(e) F_{10}

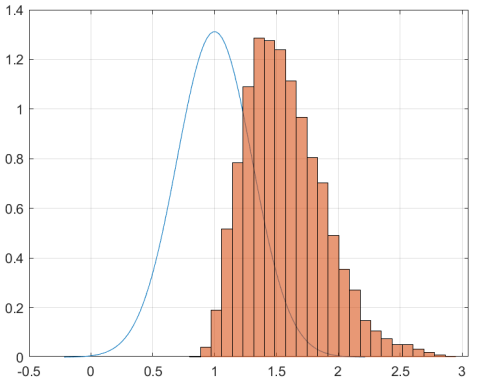

(f) F_{11}

Figure A1.4. Sampled posterior distribution of scaling parameters of forcing groups with indexes from 6 to 11. "Without priors" chain. Blue line corresponds to the the prior distribution from Smith et al. [8].

(continues)

Appendix 1. (continued)

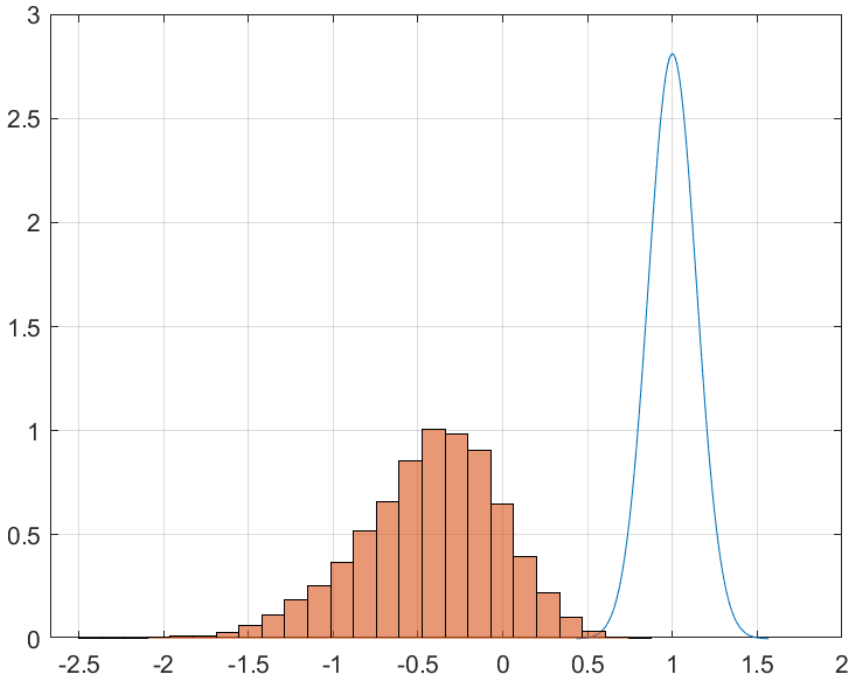

Figure A1.5. Sampled posterior distribution of scaling parameter of forcing groups number 12. "Without priors" chain. Blue line corresponds to the the prior distribution from Smith et al. [8].

(continues)

Appendix 1. (continued)

1.2 Results from the 2nd experiment ("With priors").

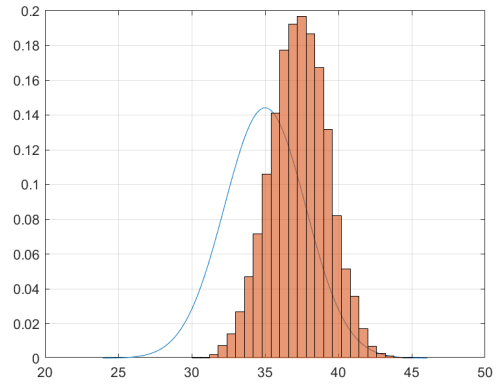

(a) r_0

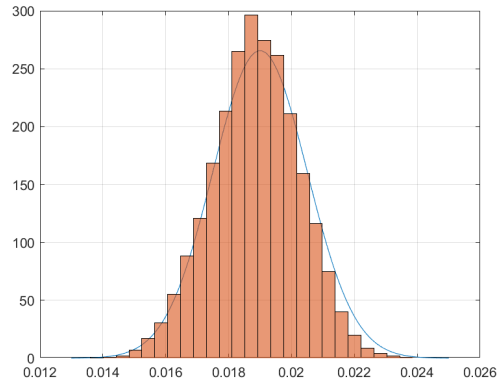

(b) r_C

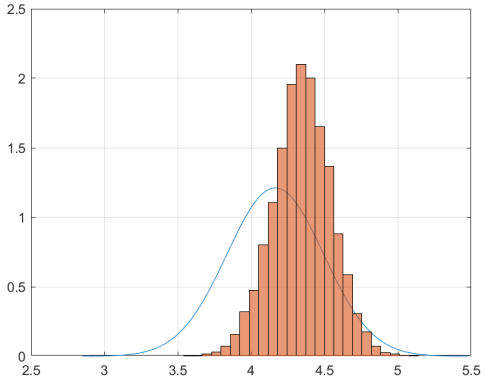

(c) r_T

Figure A1.6. Sampled posterior distribution of parameters responsible for CO_2 concentration calculation. "With priors" chain. Blue line corresponds to the the prior distribution from Smith et al. [8].

(continues)

Appendix 1. (continued)

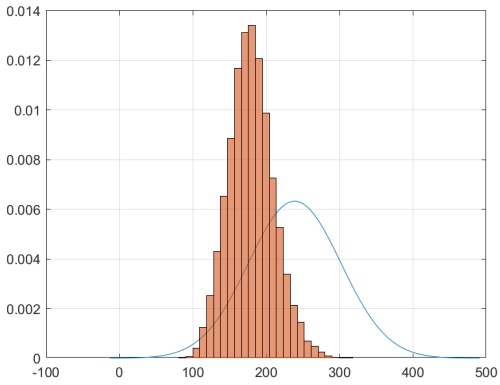

(a) d_1

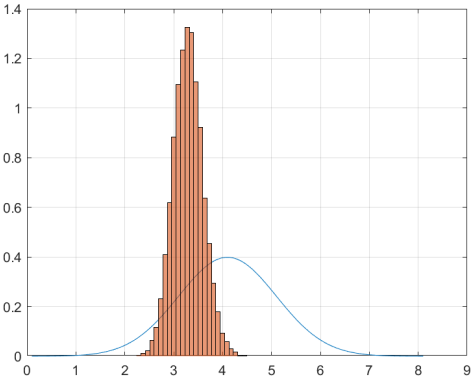

(b) d_2

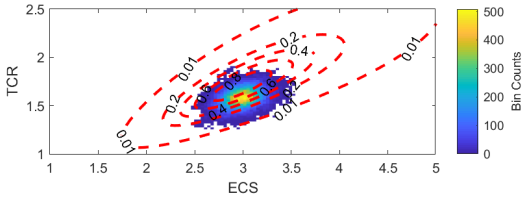

(c) TCR and ECS

Figure A1.7. Sampled posterior distribution of parameters responsible for temperature calculation. "With priors" chain. Blue line corresponds to the the prior distribution from Smith et al. [8].

(continues)

Appendix 1. (continued)

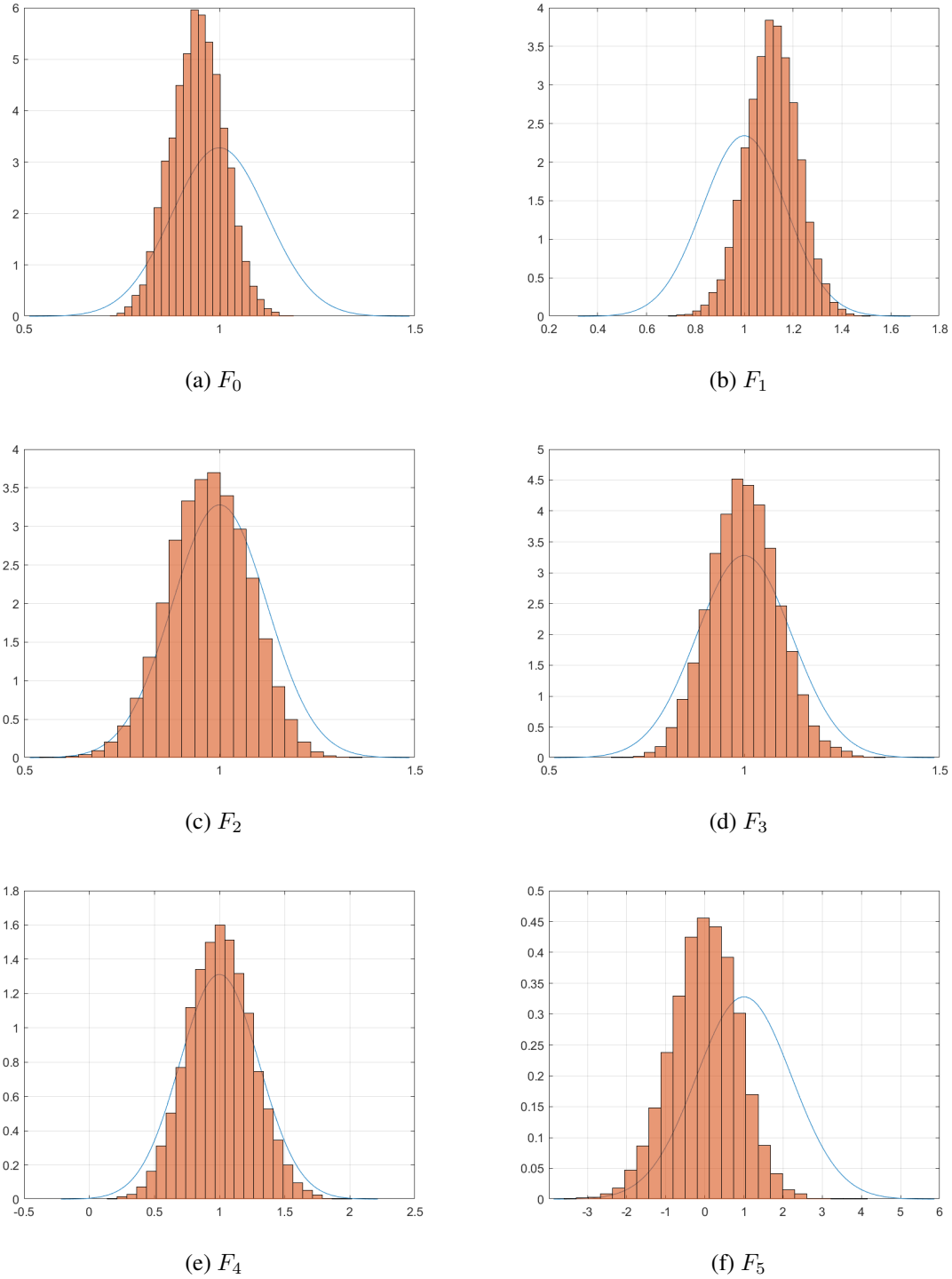

(a) F_0 (b) F_1

(c) F_2 (d) F_3

(e) F_4 (f) F_5

Figure A1.8. Sampled posterior distribution of scaling parameters of forcing groups with indexes from 0 to 5. "With priors" chain. Blue line corresponds to the the prior distribution from Smith et al. [8].

(continues)

Appendix 1. (continued)

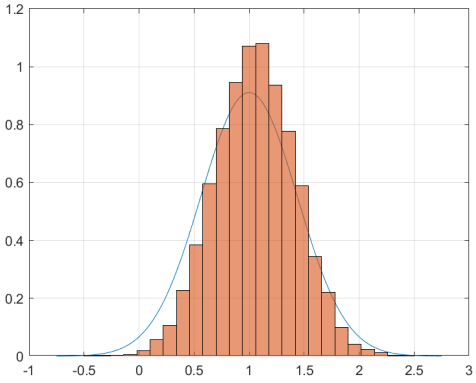

(a) F_6

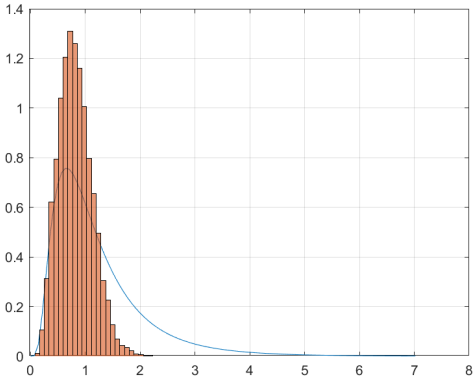

(b) F_7

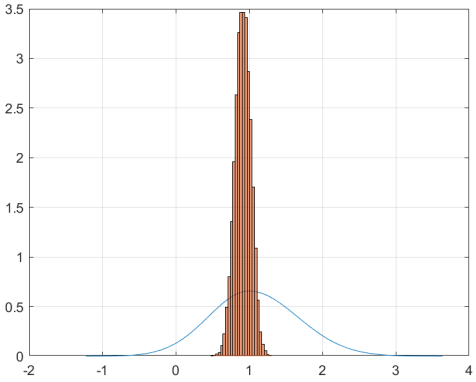

(c) F_8

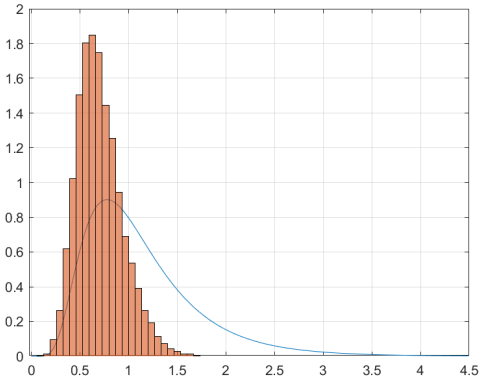

(d) F_9

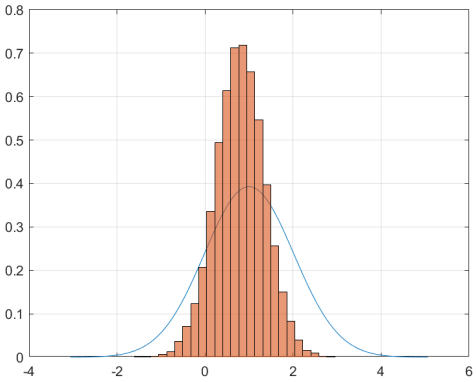

(e) F_{10}

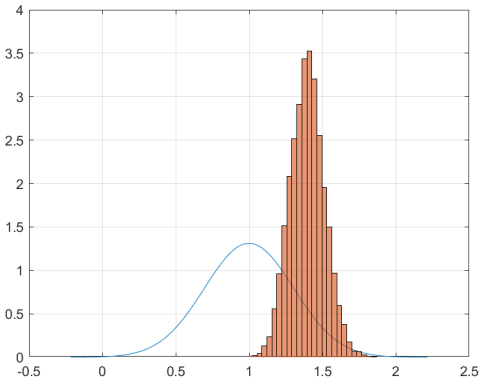

(f) F_{11}

Figure A1.9. Sampled posterior distribution of scaling parameters of forcing groups with indexes from 6 to 11. "With priors" chain. Blue line corresponds to the the prior distribution from Smith et al. [8].

(continues)

Appendix 1. (continued)

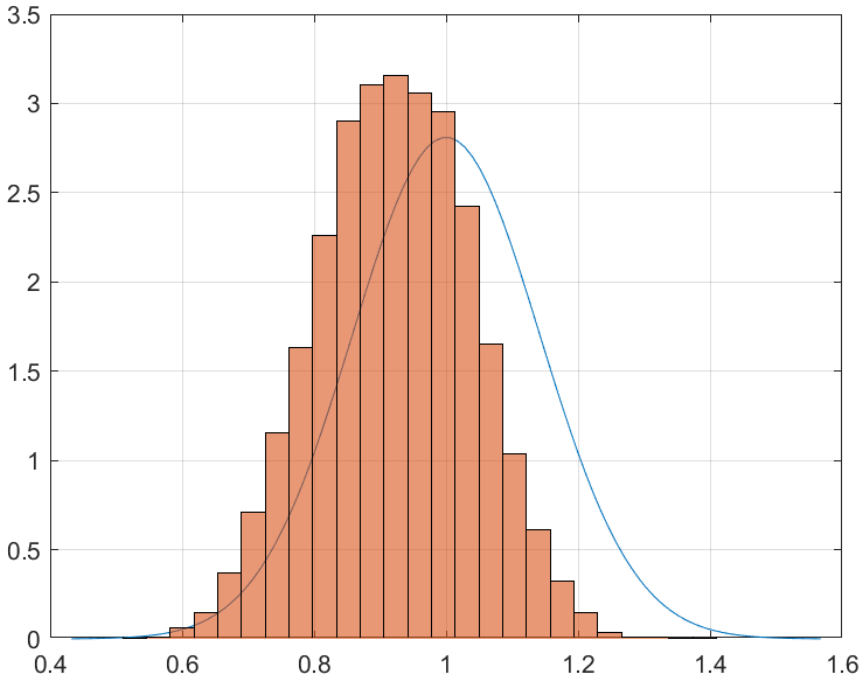

Figure A1.10. Sampled posterior distribution of scaling parameter of forcing groups number 12. "With priors" chain. Blue line corresponds to the the prior distribution from Smith et al. [8].

(continues)

Appendix 1. (continued)

1.3 Results from the 3rd experiment ("With bounds").

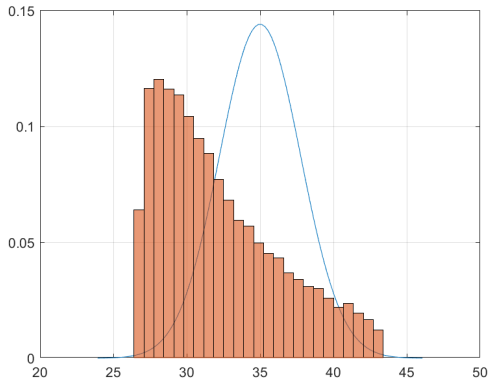

(a) r_0

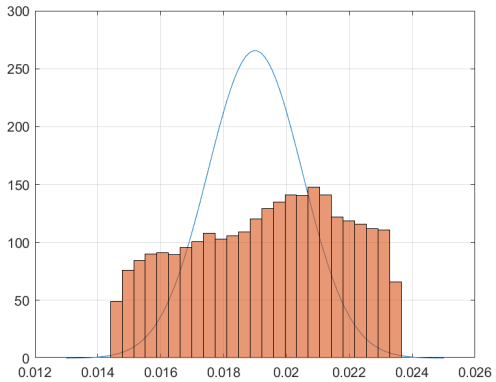

(b) r_{C}

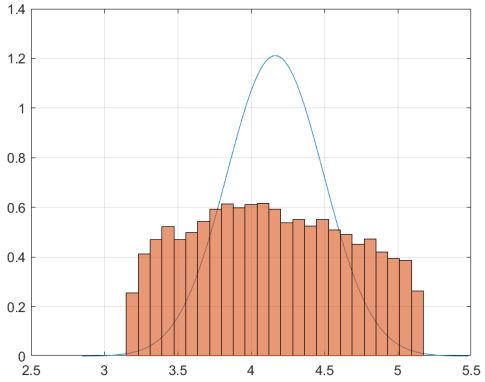

(c) r_{T}

Figure A1.11. Sampled posterior distribution of parameters responsible for CO_2 concentration calculation. "With bounds" chain. Blue line corresponds to the the prior distribution from Smith et al. [8].

(continues)

Appendix 1. (continued)

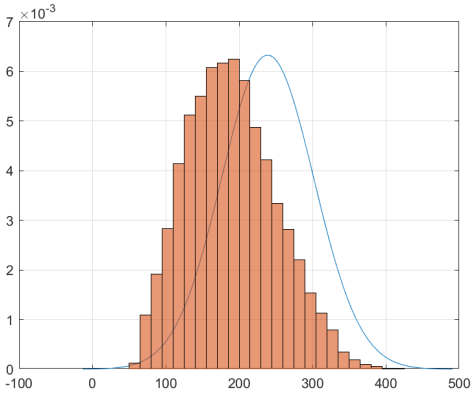

(a) d_1

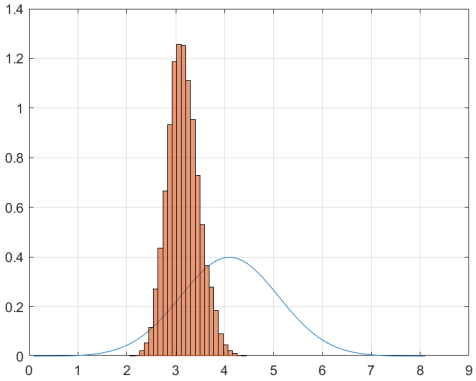

(b) d_2

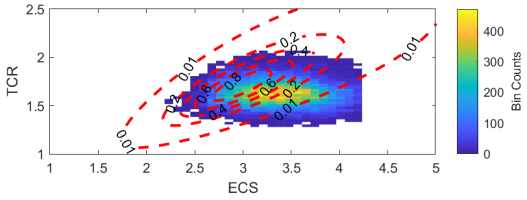

(c) TCR and ECS

Figure A1.12. Sampled posterior distribution of parameters responsible for temperature calculation. "With bounds" chain. Blue line corresponds to the the prior distribution from Smith et al. [8].

(continues)

Appendix 1. (continued)

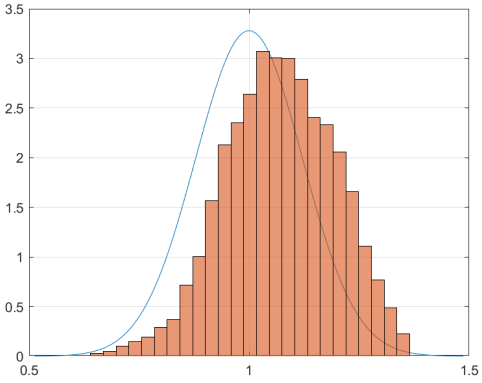

(a) F_0

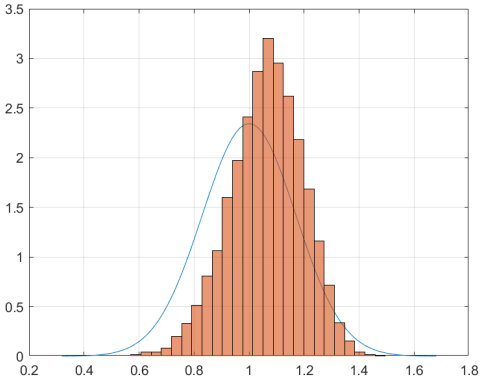

(b) F_1

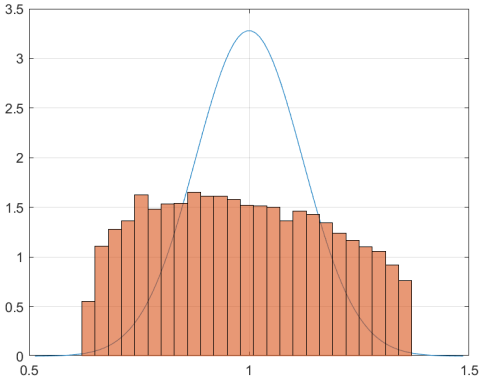

(c) F_2

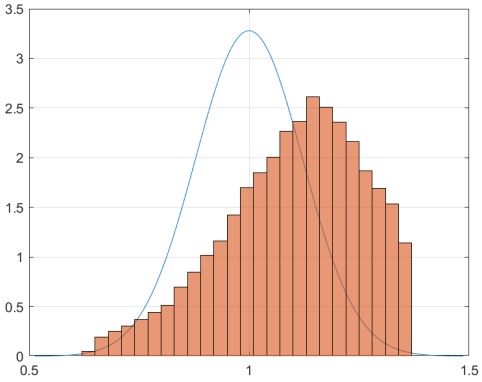

(d) F_3

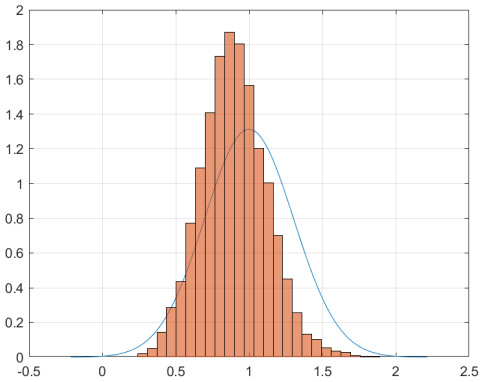

(e) F_4

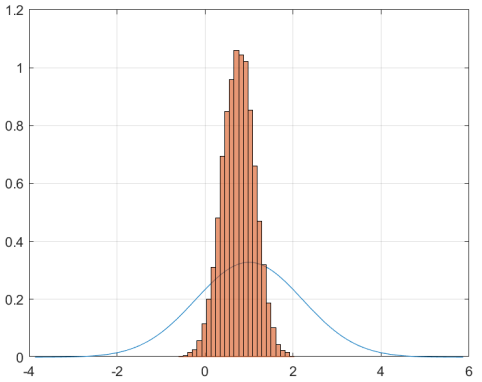

(f) F_5

Figure A1.13. Sampled posterior distribution of scaling parameters of forcing groups with indexes from 0 to 5. "With bounds" chain. Blue line corresponds to the the prior distribution from Smith et al. [8].

(continues)

Appendix 1. (continued)

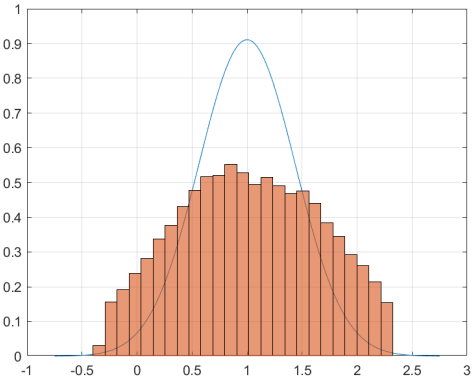

(a) F_6

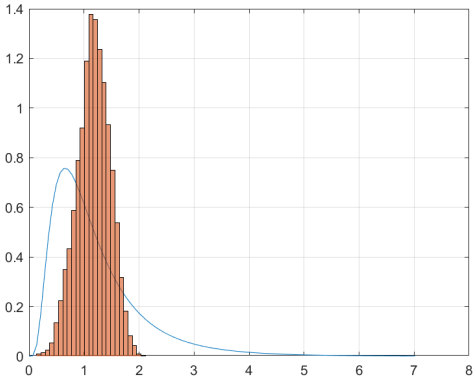

(b) F_7

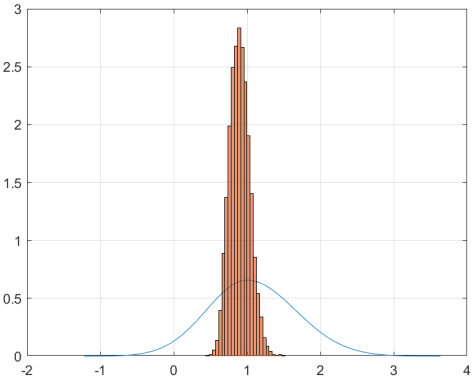

(c) F_8

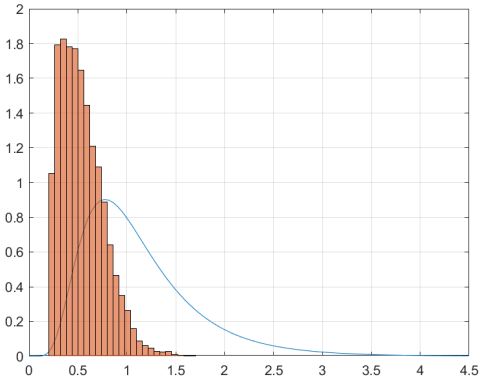

(d) F_9

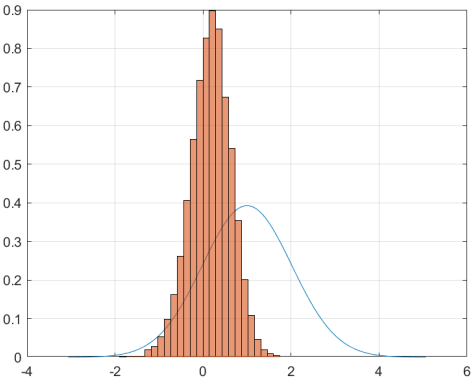

(e) F_{10}

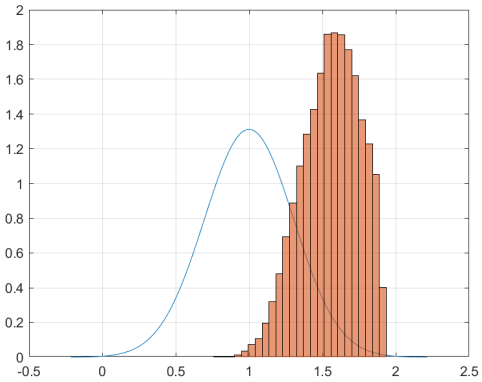

(f) F_{11}

Figure A1.14. Sampled posterior distribution of scaling parameters of forcing groups with indexes from 6 to 11. "With bounds" chain. Blue line corresponds to the the prior distribution from Smith et al. [8].

(continues)

Appendix 1. (continued)

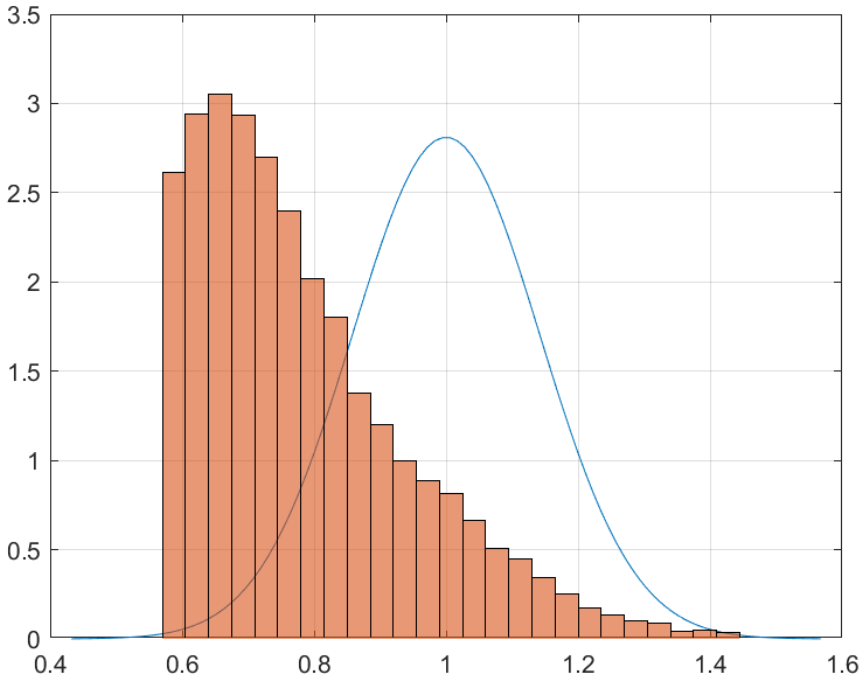

Figure A1.15. Sampled posterior distribution of scaling parameter of forcing groups number 12. "With bounds" chain. Blue line corresponds to the prior distribution from Smith et al. [8].

(continues)